Water at Interfaces

by

Oliviero Andreussi

Classe di Scienze

Perfezionamento in Chimica

SCUOLA NORMALE SUPERIORE

January 2008

Thesis Supervisor:

Prof. Michele Parrinello

Contents

Introduction

Predicting the structure of molecular solids is of fundamental importance in many scientific fields. Still it is very difficult to have reliable results, since it is a typical complex problem that cannot be easily approached with present day theoretical models. Even when a single molecular bulk solid is investigated, it is rather difficult to calculate the phase diagram, to simulate phase transition and to reproduce phase boundaries: time scales and length scales associated with these aspects are too large to be treated with *ab-initio* and classical Molecular Dynamics (MD). On the other hand, when one is interested in non homogenous systems, like the ones presenting interfaces between a molecular solid and the vacuum and/or between two different solids, the problem become even more complex. It is a typical example of multiscale problem: chemical reaction that can happen at the interface can only be treated with *ab-initio* theories, but the establishing of long-range ordered structures is affordable only by using classical MD. On the other hand this latter technique is not advanced enough to treat phase transitions of reliable systems. In this thesis I will present calculations that span all these fields: in Part I the non-equilibrium dynamics and structure of interfacial ice on a chlorine terminated Si(111) surface will be examined; in Part 2 the structure of the water overlayer at the Pt(111) surface will be

analyzed.

Despite the intrinsic multiscale nature of the problem, in many cases it is possible to focus only on part of the problem, neglecting or approximating the remaining parts. This approach is widely adopted in the present work: its limitations and its advantages form an important part of the obtained results. In particular in the first part of this thesis we ruled out the possibility of chemical reaction at the interface between water and the substrate, and we used *ab-initio* simulations only to model a classical interaction potential (force-field). This was used throughout in classical MD simulation to analyses the structure and phase transitions of thin films of interfacial water. On the other hand, in the second part of this thesis we limited our analysis to the first water overlayer on top of the Pt(111) surface, and we studied the relative stability of different structures, both intact and dissociated. For this purpose we used extensive *ab-initio* calculations, but the dimension of the system and the accuracy of the calculations limited the possibility to model complex reconstruction and to asses the stability of the different structures at finite temperature.

Part I

Non-equilibrium dynamics and structure of interfacial ice

Chapter 1

Introduction

The characterization of interfacial molecular assemblies of nanometer scale is of fundamental importance to chemical and biological phenomena [1–4]. For water the characterization of interfacial systems is even more important, since it is a key issue in a rich variety of phenomena, including those in electrochemistry, heterogeneous reactions and tribology. Nonetheless the directional molecular features of the hydrogen bonding and the different possible structures, ranging from many different crystal phases to amorphous phases, enormously increase the complexity of the problem. Experiments are, in most cases, not able to give a direct and detailed molecular picture of the interfacial structure. Most of the times experimental techniques give information only about few aspects of the system: the interpretation of those information, when is not biased by the scientist's expectations, need to be supported by theoretical models and calculations. Nonetheless, due to the high complexity of the problem the same informations fit often well in completely different structures, giving rise to long debates in the literature (see for example the discussions in Part

II for the case of metal-water interfaces).

The development of a new ultrafast electron crystallography (UEC [5–8]) was able for the first time to shed light on the microscopic structure of interfacial ice with a very high spatial and time resolution [9]. By exploiting such a technique, C.-Y. Ruan et al. were able to extend the methodology to study also non-equilibrium processes occurring after a sudden temperature jump of the substrate [9]. The variety and the complexity of their experimental results were able to give a picture of the system close to complete. Still a detailed microscopic characterization was missing and it was strong the need for a theoretical model to explain in details the features of the system.

The absence of chemical reaction in the system (as verified by the reproducibility of the experiments [9]), the long timescales of the experiments (1ns) and the need of simulating big system sizes in order to reproduce phase transitions in a reasonable way, all these elements contribute to the choice of classical Molecular Dynamics (MD) as the main investigation tool. Nonetheless, some *ab-initio* calculations have been done, in order to get general information on the properties of the system under study and to parametrize the classical interaction potential (force-field): while for bulk silicon [10–17] and the water molecule [18–20] many different classical force-fields have been extensively developed, as far as we know no classical MD study of the silicon-chlorine surface has been previously reported.

In Chapter 2 the experimental findings obtained on interfacial ice on a silicon substrate, both about the structure and the non-equilibrium dynamics, are resumed. In Chapter 3 the experimental and theoretical literature about the substrate and the water-

substrate interaction is described. In Section 3.1.3 and 3.2.2 of this Chapter some *ab-initio* calculation on small systems are reported and reviewed: these results are used to parametrize a classical force field to be used in Classical Molecular Dynamics simulations (Section 3.1.4 and 3.2.3). Finally, Chapter 4 and 5 report the Classical Molecular Dynamics calculations of the structure and of the non-equilibrium dynamics respectively.

Chapter 2

The experiments

2.1 System preparation and characterization

The substrate of the system under study is composed by a single crystal Si(111) surface terminated chemically with chlorine atoms. The surface preparation follows a standard [21] wet chemical scheme that produce a regular reconstruction with chlorine atoms chemisorbed on atop sites. Even if the surface is demonstrated to be not strongly interacting with water (see [9, 22] and the theoretical calculations in Chapter 2), the charge separation between silicon and chlorine atoms renders the interaction stronger than with typical hydrophobic surface, such as hydrogen terminated silicon surfaces or platinum [9, 23, 24]. This 'non hydrophobic' interaction is demonstrated by contact angle measurements [9]. Before dosing with water, the surface geometry is characterized by means of reflective high energy electron diffraction (RHEED). By rotating the crystal, the rocking curves and the dependence of the diffraction pattern on the incidence angle are obtained (as shown in Fig. 2.1).

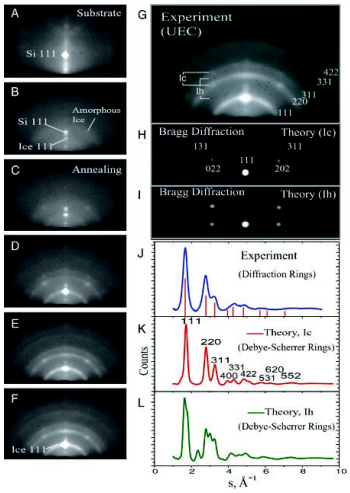

Figure 2.1: (**A** to **F**) The process of in situ growth of ordered ice is illustrated through vapor deposition of water on a cold (110 K) silicon substrate. The adsorption of water on the substrate is seen from the disappearance of 111 Bragg spot of silicon (**A**) and from formation of 111 Bragg spot of crystalline ice, together with the diffraction rings of amorphous ice (**B**). Annealing promotes the formation of long-range crystalline structure, as shown in the increase of the brightness of the spots and sharpening of the rings (**C** and **D**). The structures stabilize as the diffraction shows nearly no change in the rings, spots and streak (**E** and **F**). (**G** to **I**) Experimentally observed diffraction and simulations of spots from a nanometer-thick substrate, orientated cubic (I_c) and hexagonal (I_h) structures. Experimental (**J**) and theoretical (**K** and **L**) radially averaged diffraction intensity curves. (From Ref. [9])

Water is adsorbed on the substrate by means of vapor deposition at low temperature $T = 110$ K. The initially amorphous ice is then annealed with a temperature ramp of $\sim 2°/\,\mathrm{min}$. Crystallization from the amorphous structure starts near 140 K and reaches its saturation at ~ 150 K with the highest degree of long-range order. The temporal behavior of the interfacial ice structure is monitored by electron diffraction. RHEED patterns clearly show the appearance of a diffraction spots with the same scattering angle of the (111) silicon spot but at shorter values of the momentum transfer coordinate. The observed Bragg spot indicates that water molecules are oriented by the substrate with a long-range order. As annealing proceeds the intensity and the sharpness of the spot increase together with the appearance of sharp diffraction rings. The positions of the rings coincide with the spots in the reciprocal lattice and these rings indicate the emergence of crystallite structures, locally ordered but disordered relative to each other. By comparing the position of diffraction patterns, both spots and rings, with the one of ideal hexagonal and cubic Ice it is possible to identify the cubic phase as the dominant one. From the position of the Bragg peaks the interplanar distances in the interfacial ice were determined to be as long as 3.80 ± 0.23 Å, 2.27 ± 0.15 Å and 1.93 ± 0.07 Å for the (111), (220) and (311) planes respectively. These results are consistent with reported powder diffractions of cubic structure. From the symmetry and positions of Bragg spots it is possible to identify that the long-range ordered interfacial structure is rotated by 30° with respect to the substrate lattice. Thus the two dimensional surface unit cell of water can be described as a superlattice $\left(\frac{2}{3}\sqrt{3} \times \frac{2}{3}\sqrt{3}\right) R30°$. In this orientation the distance between oxygen atoms in the bottom layer of water is found to be just a little longer (4.5 Å) than the distance between on-top and interstitial sites (4.43 Å) of

the chlorine layer. From the brightness and width of Bragg spots a thickness of nanometer scale is obtained for this structure.

2.2 Non-equilibrium dynamics

The most important advances of the UEC is the possibility to follow the evolution of the system with a resolution of few picoseconds. The substrate is heated with an ultrafast infrared (IR) laser pulse (800nm, 120fs long). A weaker beam is split from the IR beam, frequency tripled, and focused on a photocathode to generate the electron pulses. These pulses, $\lambda = 0.07$ Å at 30 keV, are directed into the system surface in a reflection geometry (incidence angle $\theta_i < 1°$). After diffraction, the pulses are collected by a charge-coupled device (CCD) camera assembly capable of single-electron detection. The results are plotted as difference images with respect to the diffraction pattern at the beginning of the laser pulse. The experiments are repeated using different values of the intensity (fluence) of the IR laser pulse.

From the experiments it comes out that both the interfacial ice and the crystallite islands undergo a sudden reorganization of their structures after the temperature jump (as shown in Figure 2.2). Nonetheless the two water systems present different characteristic timescales, in particular the interfacial ice having a less prompt response ($\sim$ 35 ps with respect to $\sim$ 5 ps, see Figure 2.3). Since water does not absorb the IR light of the laser pulse, this relatively fast response of the layered ice signifies the high efficiency of heating by nondiffusive vibrational coupling. For this reason, the presence of a higher energy barrier for the interfacial ice was suggested. Moreover, the depletion of the old diffraction pattern (both

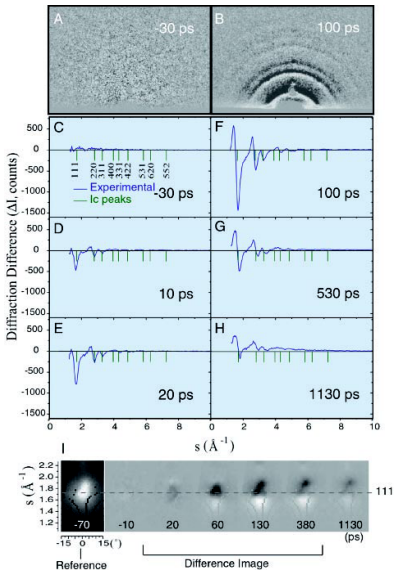

Figure 2.2: (**A** and **B**) Diffraction difference images at negative (-30 ps) and positive (100 ps) times. The reference time is at -70 ps. (**C** to **H**) The radially averaged diffraction difference intensity curves at several delay times [(**C**) -30 ps, (**D**) 10 ps, (**E**) 20 ps, (**F**) 100 ps, (**G**) 530 ps, (**H**) 1130 ps] show the structural dynamics for layered crystallites at substrate energy fluence of 22 mJ/cm^2. (**I**) The diffraction difference images for the 111 Bragg spot. The vertical axis si the momentum transfer coordinate in the reciprocal space and the horizontal axis is the azimutal scattering angle. (From Ref. [9])

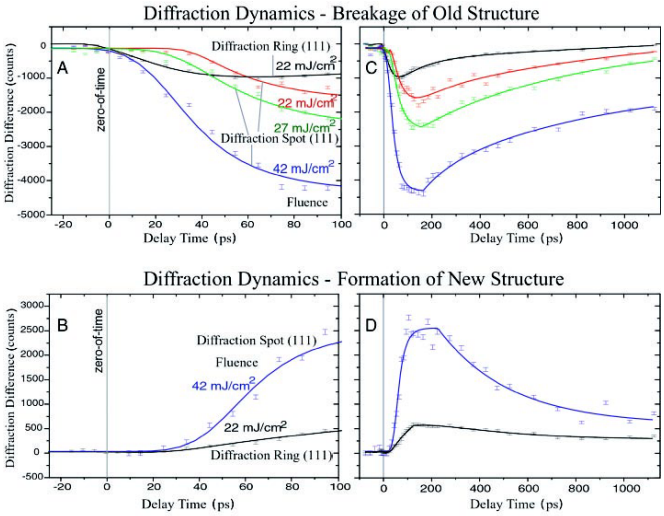

Figure 2.3: Temporal evolution of diffraction gated in the 111 reflection region. (**A**) The early-time ($\leq$ 100 ps) depletion of old 111 diffraction spot and ring at several energy fluences. (**B**) The formation of a new 111 diffraction spot and ring, also at early times. Note the apparent delay with respect to the zero-of-time, which is independently determined with uncertainty of 3 ps. The corresponding changes at longer times are shown in (**C**) and (**D**). (From Ref. [9])

spots and rings) was followed by the formation of a new structure that was characterized in terms of a differential radial distribution function. This structure presents an elongation of the hydrogen bonds between water molecules and it has a slow rate of diffusion (slower of the experimental timescale). Thus, at the end of the experiments (1 ns) the system has only partially recovered its original structure.

Chapter 3

The interaction potential

3.1 Characterization of the substrate

3.1.1 Experimental results

The interaction of chlorine with silicon surface is of interest in pure and applied physics. In contrast with many other adsorbates, chlorine has well ordered overlayers on semiconductor surfaces. Especially the chemisorption on Si(111) has been the subject of various experimental [25–31] and theoretical [25,27–29,32–42] investigations and has become a prototype system for studying the interaction of adsorbates with semiconductor surfaces. The adsorption is the first step of the reaction of chlorine with the solid silicon and is also of importance for the interpretation of the reaction process that occur during plasma etching and chemical vapor deposition.

The chlorine terminated silicon (111) surface was first investigated in detail in the late seventies in the context of chemisorption on semiconductor surfaces. While the evidence

of a 1×1 surface structure was clear from Low-energy electron-diffraction studies [43,44], the preferred site of adsorption was the subject of debate in the literature, especially due to an apparently different adsorption mechanisms in different silicon surface reconstructions and between Si and Ge [25, 26, 30, 34, 36]. Two possibilities were considered, covalent binding to the top silicon atoms and ionic binding with the chlorine in a threefold site. Because of the large adsorbate-substrate electronegativity difference a threefold-coordinated-site geometry is probable and has been widely used for halogens chemisorbed on metal (111) surfaces. In this geometry the Si broken-bonds electrons can be used to complete the closed-shell noble-gas configuration of Cl^{-1}. On the other hand, if electronegativity differences are not the dominant factors one would expect the onefold-coordinated covalent-site geometry (atop) to be correct. The use of photoemission spectroscopy [25–28] and x-ray absorption measurements [30], together with some of the first pseudo-potential *ab-initio* calculations [25, 27, 32], lead to a detailed description of the surface structure, in which chlorine atoms are chemisorbed on atop positions. These experiments and *ab initio* calculations give a detailed picture of the electronic structure of the chlorine terminated Si(111) surface; they are also in good agreement with each other. From those results a silicon chlorine bond length of 2.03 ± 0.03 Å was obtained [30, 36]. More recent high resolution electron energy loss spectra (HREELS) gave an estimate of the silicon-chlorine bond strength, characterized by a stretching frequency ranging from 560 to 588 cm^{-1} [22, 45]. Successive HREELS studies indicate that the Si-Cl stretching mode is affected by chlorine coverage: a shift of the frequency from 600 cm^{-1} to $\sim$ 550 cm^{-1} has been reported in experiments [46] using different values of Cl exposure and on heating the systems (thus increasing chlorine

desorption).

The first chlorine terminated silicon (111) surfaces were produced by gas phase reaction between molecular chlorine and a cleaved silicon surface under ultrahigh vacuum conditions and UV irradiation [47] and/or at high temperature [48, 49]. Nonetheless, the increasing interest in this kind of functionalized semiconductor systems have lead to the development of different alternative techniques. In particular, the possible application of these surfaces as intermediate in Si(111) functionalization reaction (e.g. to create alkyl terminated silicon surfaces) [45], has lead to the devise of alternative wet chemical pathways [21, 22, 45, 50]. Even if the final surface has the same structure, the level and kind of impurities are different using different methods of preparation [22, 50]. In particular, for the surface prepared with solution phase reaction, a small presence of adventitious O on the surface has been pointed out experimentally [21, 22, 45]. Nonetheless, for the purposes of this work we shall neglect the influence of this impurities.

As for the stability of the surface, the chlorine atoms do not chemically interact with water molecules and the surface is stable under water vapor exposure [22]. However it was shown that the substrate is unstable upon dipping the sample into water and under long air exposure as well [22]. The reported reaction mechanism seems to involve oxygen insertion into the Si-Si backbonds followed, in a second step, by the replacement of the terminal Si-Cl with either terminal H atoms or OH groups. In the present work we shall assume that the influence of O absorption is minimal and we shall neglect it. Similarly, we rule out the possibility of a substrate-water chemical reaction during the ultrafast heating, as experimentally supported by the full reproducibility of the distinctive diffraction features

for many runs of laser annealing and adsorption-deposition cycles.

3.1.2 Theoretical results

The increasing interest in the characterization of the product of halogen chemisorption on semiconductors has been constantly followed by theoretical works. The chlorine terminated silicon surface has been studied on periodic systems [25, 27, 32] and on clusters [35, 37, 38, 40–42], with tight binding, Hartree-Fock, LDA and GC DFT with and without pseudo-potentials. The results agree on the identification of the atop silicon atom as the most stable absorption site. They also give the same qualitative picture of the electronic structure of the system: the addition of chlorine to the surface creates bands that can be attributed to the chlorine σ and π orbitals . The presence of a partial double bond between the chlorine atom and the atom silicon atom has been inferred by calculations using different methodologies. This result is coherent with the experimental Si-Cl distance, that is much shorter than the sum of covalent radii of the two species ($\sim$2.15 Å).

Also electronic states characteristic of the first two layers of the silicon atoms are modified by the presence of the adsorbate. Nonetheless, all the theoretical works agree on the local nature of the surface bonds, as demonstrated in particular by population analysis and real-space representation of local density of states. For this reason most of the calculation in the literature have been performed on cluster systems and the consistency of the results with the cluster size is another implicit check of the local nature of the surface bonds [35]. However, it has been only recently pointed out that calculation of the Si-Cl stretching frequency is strongly sensitive to the chemical environment: in particular, the presence of dipole-dipole coupling between Si-Cl oscillators was seen to shift the Si-Cl fre-

quency to higher values [41]. Indeed, this effect is able to explain the experimental coverage dependence of the stretching frequency [46]. Moreover none of the previous theoretical works were able to reproduce the experimental stretching frequency value.

The improvements in the computational and theoretical methods allowed the calculation of bonding energies, bond lengths and population analysis in good agreement with experimental results. The use of pseudo-potentials to treat core electron was demonstrated to be a good approximation, in comparison with all electron calculations [38]. The inclusion of polarized basis sets (including d function for heavy atoms) was shown to be essential in order to reproduce the experimental bond length and bonding energy [36,38]. The inclusion of correlation effects was demonstrated to be of secondary importance [38]. On the other hand, Mulliken population analysis gave almost the same results for different methods and using different basis sets [38]: a net charge on chlorine atoms of ~ -0.3 has been obtained, with a corresponding (slightly smaller) positive charge on the topmost silicon atoms.

3.1.3 *Ab initio* simulations

In order to parametrize a classical interaction potential to be used in Classical MD simulations, some *ab-initio* simulations have been performed on the system. Calculations were done both on a cluster system and on a periodic system.

The former is the $Si_{28}Cl_6H_{30}$ cluster reported in Figure 3.1, representing four silicon layers and one chlorine overlayer. According to the standard embedding procedure, hydrogen atoms have been added in order to saturate the silicon dangling bonds. Calculations were performed at the Hartree-Fock (HF) level of theory with a 6-31+g basis set. The Gaussian 03 program was used throughout [51]. The system was first geometry-optimized

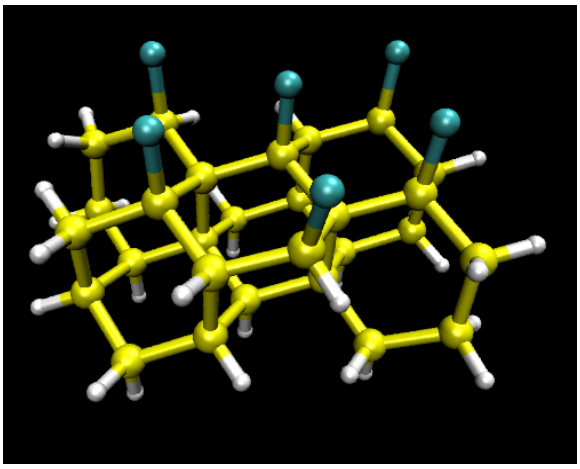

Figure 3.1: Structure of the $Si_{28}H_{30}Cl_6$ cluster used for the *ab-initio* calculations. Si/Cl/H atoms are depicted as yellow/blue/withe spheres respectively.

and then Mulliken population analysis and ESP charges were computed.

For the periodic system, calculations have been performed with the CP2K suite of programs [52]. In the framework of the Density Functional Theory (DFT) [53, 54], the BLYP [55, 56] functional was used with the DZVP double zeta basis set [52] and the Goedecker-Teter-Hutter (GTH) [57, 58] pseudo-potential to treat core electrons. The stretching frequency for the Si-Cl bond and the Wannier centers were calculated using the CPMD program [59] still exploiting DFT with the BLYP functional and an energy cutoff of 70 Ry and Martin-Troullier pseudo-potentials [60]. In both cases the $\left(2\sqrt{3}\times 2\right) R30°$ orthorhombic cell reported in Figure 3.2 and containing four silicon layers and one chlorine overlayer was considered in a three dimensional periodic boundary environment. The vertical axis was chosen to be as large as 25 Å in order to reduce the interlayer interaction along z.

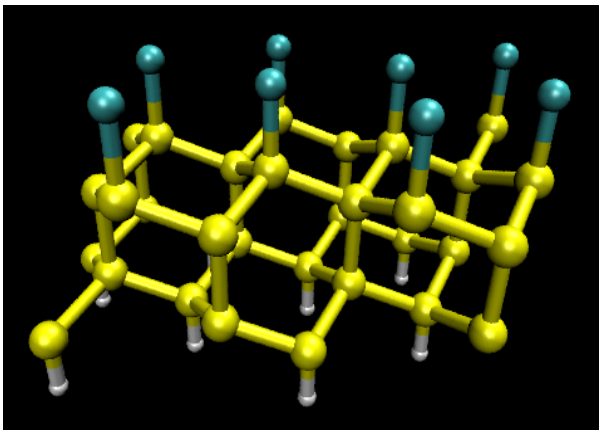

Figure 3.2: Structure of the orthorhombic cell of the analyzed substrate used in the *ab-initio* calculations. Si/Cl/H atoms are depicted as yellow/blue/withe spheres respectively.

3.1.4 Parametrized force field

Since silicon atoms away from the surface have zero net electrostatic charge, they are not supposed to directly interact with the water molecules and they can be treated in a simplified and computationally inexpensive manner. Thus, just few (four) layers of silicon atoms have been considered and the interaction between the atoms have been modelled by the Keating potential [10]. This potential includes only nearest-neighbors interactions in the form of two and three body terms and reproduces the main structural and dynamic properties of bulk silicon.

As for the topmost layer of silicon atoms and the chlorine atoms, the force field has been modelled using *ab-initio* data. The charge separation between silicon and chlorine atoms, leading to the non-hydrophobicity of the substrate, has been modelled with two point charges, of opposite sign and modulus q, centered on the two different kind of surface atoms. In order to obtain a realistic value of q, different procedure have been exploited starting from *ab initio* calculation both on the cluster system and on the periodic system.

As for the cluster system, from the calculated ESP charges, RESP charges have been calculated following the standard procedure and exploiting the AMBER suite of programs [61]. Nonetheless the distorted geometry and the non equivalence of the different Si-Cl bonds lead to a significant spread of the obtained values ($0.24e < q < 0.33e$).

As for the periodic system, first we have attempted to fit the electrostatic potential above the slab (thus away from the atomic region that is not relevant for the interaction with water molecules) with a classical electrostatic potential generated by the point charges and calculated using the Ewald sum method. Also in this case, the procedure does not give an exact estimate of the charge separation, mainly because of the 2D symmetry of the system, that lead to an almost constant electrostatic potential, and due the impossibility of neglecting the effect of the dipole on the opposite surface, where the dangling bonds of silicon atoms have been terminated with hydrogen atoms. Because of these reasons, the only result obtained by the fitting procedure is a relationship between charges on the two opposite surfaces: $q_{Cl} = q_H \cdot \frac{d_H}{d_{Cl}} + q_0$, where $d_H = 1.5$ Å and $d_{Cl} = 2.1$ Å are the mean values of, respectively, the Si-H and Si-Cl bonds, while $q_0 = 0.08e$ is the result of the fit and represent the charge separation of the whole system. Other standard procedures to calculate electrostatic charges on a periodic system suffer for the same kind of problems, and also using Wannier centers only the dipole moment of the whole system can be unambiguously determined ($\mu = -1.44D$).

From the above results, and in particular from the mean value of the RESP charges, a value of $q = 0.3$e has been chosen. To properly describe the covalent bond between silicon and chlorine atoms at the interface an harmonic potential $U^{harm}_{\mathrm{Si-Cl}} = \frac{k}{2}\left(r_{\mathrm{Si-Cl}} - r_0\right)^2$ has been

included in the force field, thus balancing the electrostatic interaction between the different point charges. From *ab-initio* trajectories, a mean distance between silicon and chlorine atoms of $r_0^{\mathrm{ab-initio}} = 2.095\,\text{Å}$ has been found, and a stretching frequency for the covalent bond of $v_{\mathrm{Si-Cl}}^{\mathrm{ab-initio}} = 575\,\mathrm{cm}^{-1}$has been obtained. Both these results are in quite good agreement with experimental and other theoretical data ($v_{\mathrm{Si-Cl}}^{\mathrm{exp}} = 560 - 585\,\mathrm{cm}^{-1}$ [22, 45], $r_0^{\mathrm{ref.\ [40]}} = 2.08 - 2.01\,\text{Å}$ [40]) and can be reproduced by using, for the harmonic oscillator parameters, values of $k = 65000\ \frac{10\,\mathrm{J}}{\mathrm{mol\,Å}^2}$ and $r_0 = 2.150\,\text{Å}$.

3.2 Substrate-water interaction

3.2.1 Theoretical results

Following the experimental paper of Zewail and coworkers [9], two different attempts to describe the interaction between water and the Si(111):Cl surface have appeared on the literature [23, 24]. Both deal with a periodic $2\sqrt{3} \times 2\sqrt{3}$ unit cell, treated at the DFT level of theory with plane-waves basis sets and pseudo-potential based codes. The interaction of a single water molecule as well as the interaction of one and more water bilayers was investigated. The results seem to suggest that the surface has a very small interaction with the water molecules [23,24]. Also the strength of a hydrogen bond between an adsorbed chlorine atom and a water molecule is demonstrated to be small, coherently with the strength of hydrogen bonds in similar systems (HCl and SiH_3Cl). In fact, the preferred orientation of a single water molecule on top of the studied surface is predicted to be the one in which the dipole of the water molecule is directed against the surface. However, given the small adsorption energies, one expects that a single water molecule can

easily go from one possible adsorption site to another and is therefore rather mobile. The energy barrier for a rotation of the molecule around the surface normal was calculated to be as low as 5 meV. This seems to indicate that a long-range ordered water adlayer as found experimentally [9] is due to intermolecular interaction rather than induced by the substrate. Similarly, the stability of an ice overlayer is demonstrated to be only due to the internal water-water interaction energy and almost not affected by the water-surface interaction. This latter interaction is shown to be larger with respect to other hydrophobic surfaces like the hydrogen terminated Si(111) surface and metal surfaces [24]. Still, the chlorine terminated silicon surface is defined to be hydrophobic and the possibility of an epitaxial growth of ice on the surface is ruled out.

3.2.2 *Ab initio* simulations

Some calculations on model systems were performed, in order to estimate the strength of the water-chlorine interaction. These calculations were performed at the GGA DFT level of theory, using the hybrid B3LYP functional, and at the MP2 level of theory. In both cases extended basis sets were used, according to previous studies of the interaction between halogens and water molecules [62]. The results of these calculations, reported in Figure 3.3 and 3.4, were also used to asses the accuracy of a periodic, plane wave and pseudo potential based calculations. The interaction is strongly dependent on the orientation, but the attractive potential has only a swallow minimum, that decrease in the case of SiH_3Cl.

Since the periodic calculations showed a good agreement with the more accurate B3LYP and MP2 calculations, the same level of theory was confidently applied to the study of the chlorine terminated silicon surface. First the interaction of a single water molecule

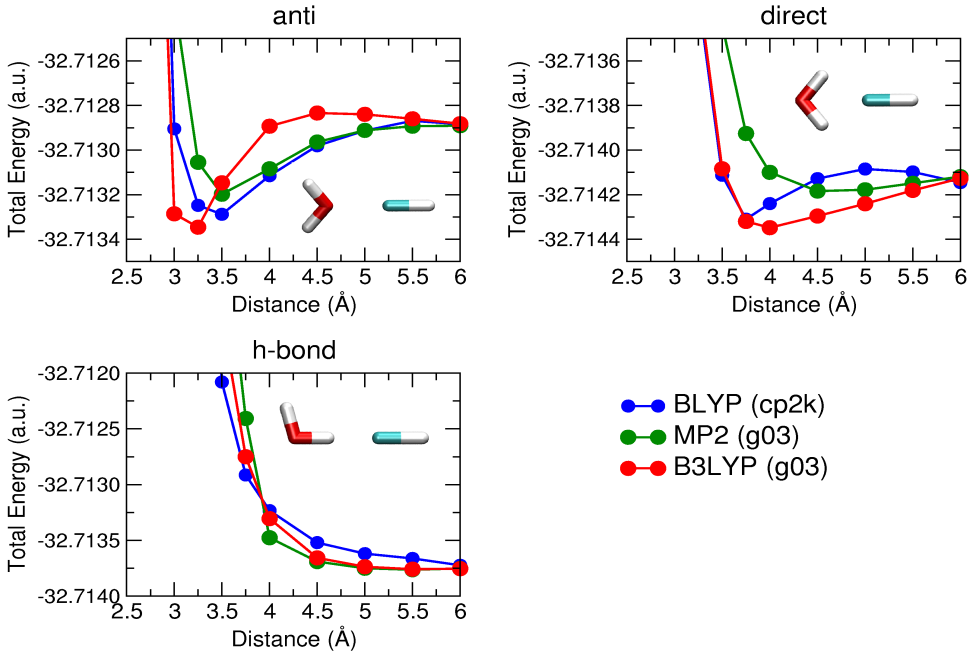

Figure 3.3: Energies of interaction between a water molecule and an HCl molecule as a function of the O-Cl separation. In the three panels, three different configurations are analyzed (anti: top left, direct: top right, h-bond: bottom). Results obtained on isolated systems at the DFT/B3LYP level of theory (red) and at the MP2 level of theory (green) are reported together with results from periodic calculations at the DFT/BLYP level of theory (blue).

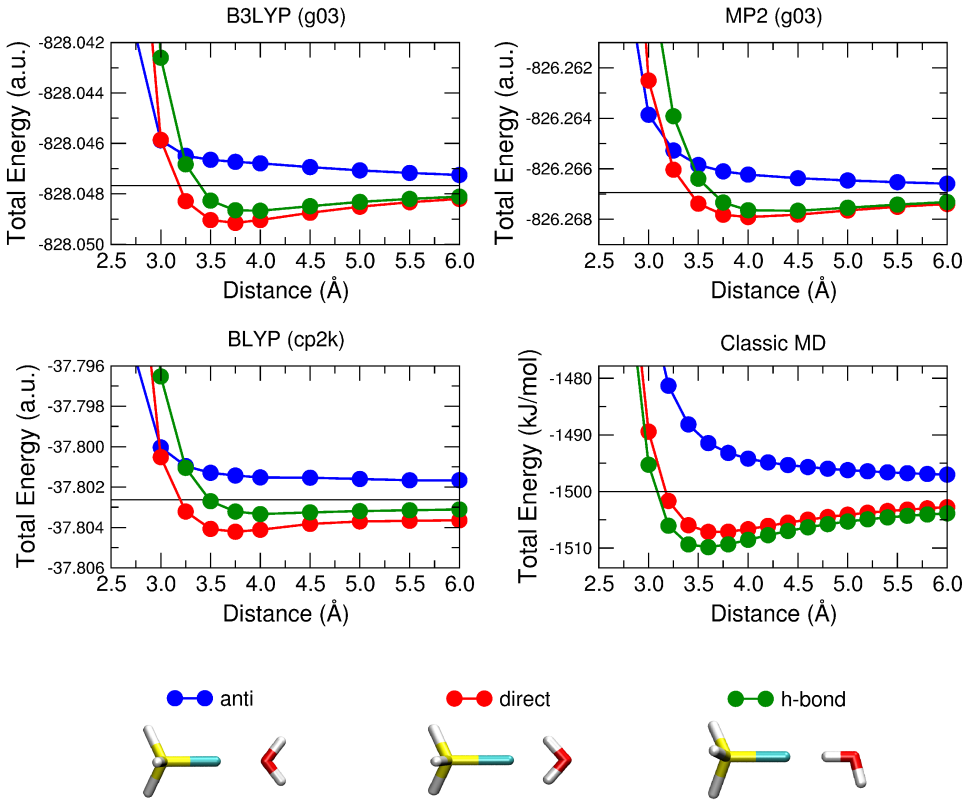

Figure 3.4: Energies of interaction between a water molecule and an SiH_3Cl molecule as a function of the O-Cl separation. Three different configurations are analyzed (anti: blue, direct: red, h-bond: green). Results obtained on isolated systems at the DFT/B3LYP level of theory (top left panel) and at the MP2 level of theory (top right panel) are reported together with results from periodic calculations at the DFT/BLYP level of theory (bottom left). As a reference, energies of non-interacting systems are represented by straight black lines. Results obtained with Classical MD exploiting the parametrized force-field (see Section 3.1.4 and 3.2.3) are reported in the bottom right panel for comparison.

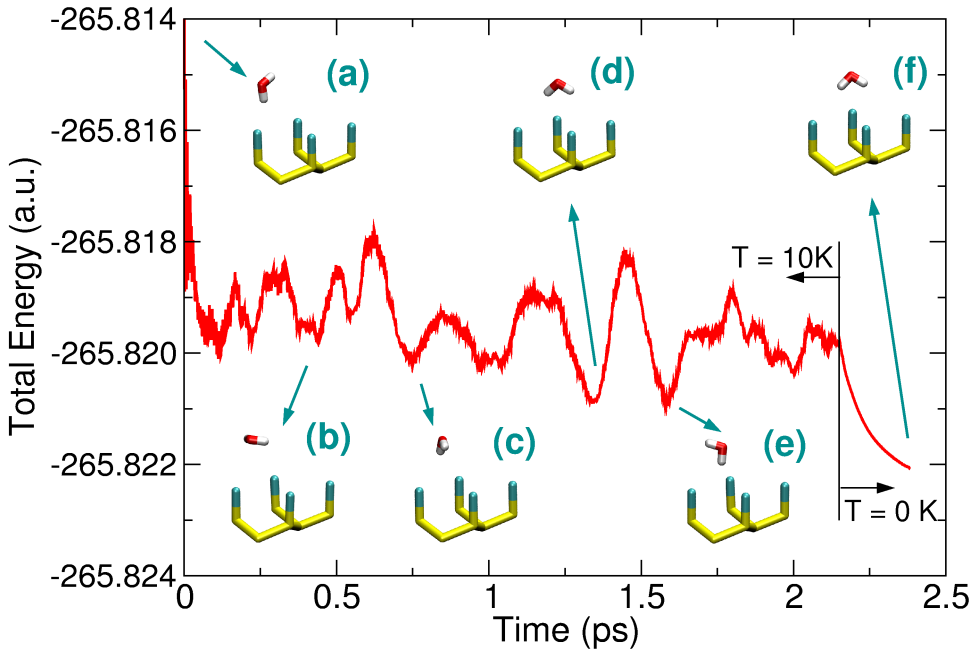

Figure 3.5: Total energy of a water molecule adsorbed on the Cl terminated Si(111) surface during an *ab-initio* MD simulation. Even at low temperature (10K) all the possible configurations are visited during the simulation time: the top site configuration (a), the flat configuration (b), the interstitial configuration (e) and some configurations with the water dipole pointing towards the surface (c),(d) and (f). These latter seem to be the minimum energy configurations, since cooling down the system to ∼0 K (last 0.2 ps of simulation) lead to structure (f).

with the surface was investigated by means of geometry optimizations and molecular dynamics at low temperature. In the former case the configurations reported in Figure 3.5 were seen to be the most stable. Nonetheless, even at very low temperature the water molecule is almost free to move and reorient itself, indicating an energy barrier between different configurations as low as few meV. Starting from the experimentally proposed top site configuration and the theoretically optimized configuration (Figure 3.5f), the behavior of the adsorption energy as a function of the water-surface distance was analyzed 3.6. When basis set superposition error (BSSE) is correctly accounted for, in both cases an overall repulsive

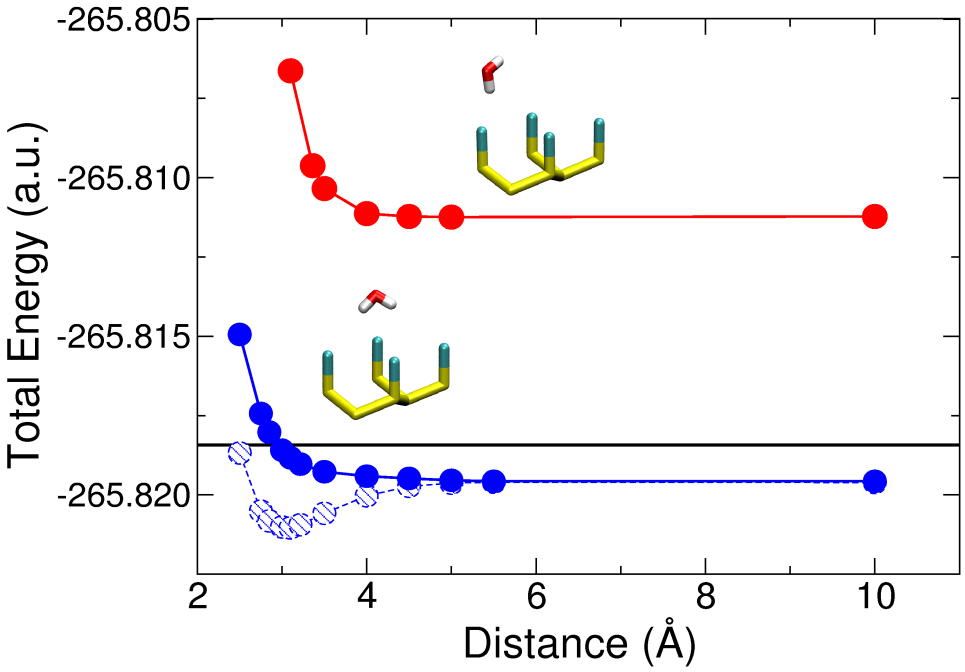

Figure 3.6: Interaction energy between one water molecule and the Cl terminated Si(111) surface as a function of the distance between the oxygen atom and the topmost surface layer. The experimentally proposed top site configuration (red) and the theoretically optimized one (blue, see Figure 3.5) are reported. As for the former, the overall interaction is repulsive and the configuration results to be unfavorable even with respect to the isolated systems (horizontal black line). As for the latter, when basis set superposition error (BSSE) is not accounted for (dashed line), an artificially attractive water-surface interaction is found for the theoretically optimized configuration. The overall BSSE corrected surface potential is repulsive, but the system is stabilized with respect to the isolated references due to the positive electrostatic interaction.

interaction if found. Contrary to the top site geometry, the configuration with the water dipole pointing towards the surface is found to be stabilized by electrostatic interaction with respect to the isolated systems (water and surface alone).

In addition, few *ab-initio* simulations have been performed in order to investigate the structure of the interfacial layers of water. The system was generated superimposing a bilayer of cubic ice (twelve water molecules) on top of the simple orthorhombic cell of Figure 3.2, according to the experimentally proposed geometry ($\sqrt{3} \times \sqrt{3}R30°$, see Figure

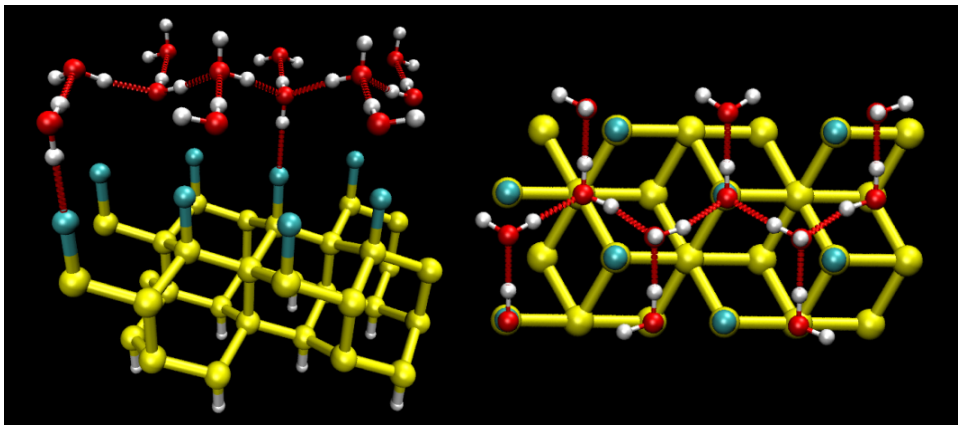

Figure 3.7: Perspective (left panel) and top (right panel) views of the structure of the orthorhombic cell used in *ab-initio* calculation to evaluate the water-surface interaction. The water molecules configuration was generated according to the experimental proposed one [9].

3.7). Different configurations of the system, with different arrangements of the hydrogen network, have been successfully optimized, but after few fs of MD simulation they start to move away from the substrate surface: it seems that the interaction energy of the surface with water molecules is too small to avoid them to leave the surface, it is just enough to let them orienting in preferable directions. In addition, the reduced dimensions and the periodic boundary conditions lead to a strengthening of the ice network, thus reducing the possibility of a constructive interaction with the substrate. Relaxing the periodicity of the system can help in preventing the system to leave the surface. Still, the main result of the calculations is that the interaction between the water overlayer and the surface is negligible.

3.2.3 Parametrized force field

Water was modelled by the four-site transferable interaction potential TIP4P [63], that is known to reproduce accurately the phase diagram of water [64, 65]. This model

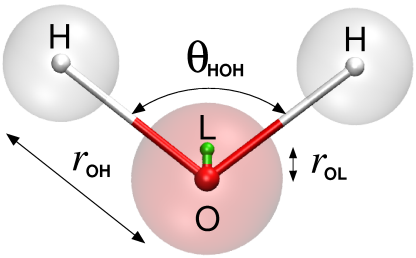

	$q_H(e)$	$\sigma_0(\AA)$	ε_0(kcal/mol)	r_{OH}	θ_{HOH}	r_{OL}
TIP4P	0.520	3.15365	0.1550	0.9572	104.52	0.15

Table 3.1: Structural representation and parameters of the TIP4P model for water. q_H represents the point charge located on the two protons. A charge equal to $-2q_H$ is located on the L site while a Lennard-Jones interaction with parameters given by σ_0 and ϵ_0 is centered on the oxygen atom.

involves three point charges located on the two protons and on a site slightly displaced with respect to the oxygen position along the C_{2v} molecular axis. A short range interaction of the Lennard-Jones (LJ) type is also included on a forth site, centered on the oxygen atom. The geometrical and physical parameters of the model are resumed in Table 3.1.

Finally a short range interaction between the surface and water molecules is introduced, using a Lennard-Jones potential centered on chlorine atoms. Since the water-chlorine interaction was proved to be negligible, the parameter of this LJ potential were chosen to be the same that applies to a single Cl^- anion in solution and they were taken from the standard Gromacs force field [66].

Chapter 4

System structure

4.1 Simulation background

The classical molecular dynamics calculations has been carried out by a modified version of the DLPOLY program [67]; simulations have been performed either in the microcanonical (NVE) or in the canonical (NVT) ensemble, the latter enforced by a Berendsen thermostat [68]. To evaluate the long range forces, two approaches have been used, depending on system dimensions: for systems with less than 500 water molecules, the Hautman Klein Ewald method [69] (precision cutoff of 10^{-4}) have been used, in which the periodicity of the system is purely two dimensional; for bigger systems, the faster Smoothed Particle Mesh Ewald method [70] (precision cutoff of 10^{-6}) have been adopted and the dimension of the cell vector perpendicular to the surface have been increased, in order to minimize the interactions between periodic replicas of the slab (the dimension of the z-axis is more than the double of the dimension of the occupied space). In all the calculations a timestep of 1.0 fs has been used.

The equilibrium properties of the system have been studied in a wide range of temperatures, from 70 K to 240 K (close to the TIP4P melting point [65]). To improve the statistics, when needed, calculations have been repeated using different initial proton disordered configurations (for crystal-like structures) or different random initial velocities (for liquid-like and amorphous structures).

4.1.1 Analysis tools

The following properties have been analyzed at each temperature:

- Bond-orientational order parameter Q_6 [71]: it is a rotationally invariant combination of bond spherical harmonics $\{Y_{lm}(\theta, \varphi)\}$, where $\theta(\vec{r}_{ij})$ and $\varphi(\vec{r}_{ij})$ are the polar angles of the bond between atom i and its nearest neighbor j, with respect to some fixed reference coordinates system. The formal expression of this quantity is given by

$$Q_l = \left(\frac{4\pi}{2l+1} \sum_{m=-l}^{l} \left| \sum_i \sum_j Y_{lm}\left(\theta\left(\vec{r}_{ij}\right), \varphi\left(\vec{r}_{ij}\right)\right) \right|^2 \right).$$

  It is a global properties of the system, and it is able to discern between liquids ($Q_6 = 0.0$) and crystals of different structures ($Q_6 \geq 0.4$). Moreover, it has been successfully used as an order parameter in different studies of ice melting and crystallization [72, 73].

- Structure factor $S(\vec{k})$: it is a measure of the translational order in wavelength space and it is the main quantity obtained from the diffraction experiments we are analyzing. It can be calculated from fluctuations in the spatial Fourier transform of the number density $\rho(k) = \sum_{i=1}^{N} \exp\left(i\vec{k} \cdot \vec{r}\right)$. From the experimental diffraction spots and rings

for the interfacial ice, the structure factor should present main peaks in correspondence of the (111), (220) and (311) vectors of the reciprocal ice Ic lattice.

- Radial distribution function $g_{\mathrm{oo}}(r)$: this function gives the probability of finding a pair of oxygen atoms at distance r apart, relative to the probability expected for a completely random distribution at the same density. This function is directly related to diffraction experimental data, since it can be obtained from a sine transform of the diffraction intensity curve (like the ones reported in Figure). Thus it is a key feature of the experiments we are simulating. In order to be as close as possible to the experimental results, the reported behaviors for the $g\,(r)$ have not been normalized by the volume element.

- Distribution function $\rho(z)$: this function represent the molecular number density at a distance z from the substrate surface. It is a generally studied quantity for systems containing interfaces or in confined geometries.

- Bivariate joint probability distribution $P(\cos\theta, \phi)$: the orientation statistics of an entire (rigid) molecule relative to an external vector can be fully described by the bivariate joint probability distribution of two independent orientational parameters. Has been previously shown [74] that an appropriate choice of the two orientational parameters involve the angular polar coordinates (θ, ϕ) of the vector X, normal to the surface, in a coordinate frame fixed to the individual water molecules. This frame is chosen in such a way that its x, y and z axes correspond to the molecular normal vector, H-H vector and dipole vector, respectively (see also Figure 4.1). With such a choice of the coordinates frame, a positive (negative) value of $\cos\theta$ corresponds to

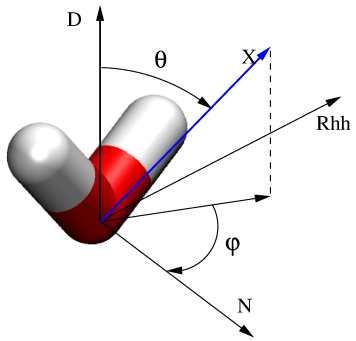

Figure 4.1: Representation of the angular polar coordinates (θ,φ) of the vector X normal to the surface in the coordinate frame fixed to a water molecule.

a water molecule with its dipole pointing towards the free surface (substrate). For a perfect crystal of interfacial ice Ic, four preferred orientation are present, while for totally amorphous ice and for liquid water a constant value for the probability distribution should be obtained. Analysis has been performed dividing the system in three regions: interface (between the substrate surface and the first-second bilayers separation), free surface (in the region above the last but one bilayer) and bulk (the water molecules between interface and free surface).

- Diffusion coefficient D: to characterize the translational mobility of the water molecules in the different regions of the film, self diffusion coefficient have been calculated from the linear behavior at long time of the mean-square displacement (MSD) of the molecular centers of mass, as

$$D_i = \frac{1}{6} \lim_{t\to\infty} \frac{d}{dt} \left\langle \left|\vec{r}_j\left(t\right) - \vec{r}_j\left(0\right)\right|^2 \right\rangle_i , \tag{4.1}$$

where $\langle\rangle_i$ denotes the averages over molecules belonging to the i-th region of the system (corresponding to the i-th bilayer in a perfect interfacial ice crystal). A water molecule

has been assigned to a particular region depending on the whole amount of time spent in it during the simulation. An analysis of the relative magnitude of the molecular mobility perpendicular ($D^{\perp}$) and parallel ($D^{\parallel}$) to the substrate surface has also been done. It is worth to mention that when one whish to calculate the diffusion coefficient of liquids in inhomogeneous regions such as interfaces, the standard Einstein relation 4.1 is not a valid approach. More complex relations can be devised [75], involving the use of virtual adsorbing periodic boundary conditions for the calculation of the molecular mobility parallel to the substrate surface. On the other hand, for the perpendicular component the standard one dimensional Einstein relation was used in the following.

- Rings statistic: as has already been done in previous studies of phase transition [76–78], in order to analyze the ice network topology we analyzed the distribution of $n-$membered rings. The rings definition used is the one of Ref [79], with nearest-neighbors defined by the presence of an hydrogen bond between two oxygen atoms. According to the definitions of Ref. [76, 80], we define the presence of an hydrogen bond between water molecules i and j by a function f_{ij} of the atomic coordinates, which is one when the molecules are bonded and otherwise tends smoothly to zero. This function is defined as the product of two terms: the first one goes from one to zero as the O_iO_j distance pass from 2.7 to 3.5, while the second differ from zero if an almost aligned configuration $Oi\mathrm{H}_kO_j$ is present for any of the k hydrogen atoms belonging to O_i or O_j.

4.2 Melting and equilibrium properties

As starting configurations, both proton ordered and proton disordered structures have been used. The former has been generated in a way to maximize the dipole moment of the whole water system along the direction perpendicular to the substrate. For the latter, a modification of the Monte Carlo method developed by Buch et al. [81] has been adopted: for each water molecule, the oxygen atom is kept fixed at the corresponding ice Ic lattice position, while the hydrogens points towards two randomly chosen of the nearest-neighbors oxygen atoms; swapping of water molecules (i.e. reorientations of the hydrogen atoms) are performed until a configuration has been obtained that obey to the ice rules; then, an importance sampling Monte Carlo simulation is performed, weighting each configuration by its electrostatic interaction energy with the substrate calculated via the Ewald sum method; finally, new configurations are generated from the old ones by randomly swapping some of the water molecules and then rebuilding the ice network. Using this algorithm, configurations of three (3BL, see Figure 4.2) and nine (9BL) bilayers thick interfacial ice have been generated, composed by respectively 432 and 1296 water molecules. Neither models fully represent the experimental findings since in the experiments three interfacial bilayers are covered by crystallite islands. Unfortunately we are not in the position to simulate such a complex system. In spite of this we believe that the 3BL system is sufficiently representative of the real structure at equilibrium. However in real systems the crystalline islands provide a sink through which heat can be dissipated during the laser induced melting. Thus the behavior of the experimental system is better understood by combining the outcome of both simulations.

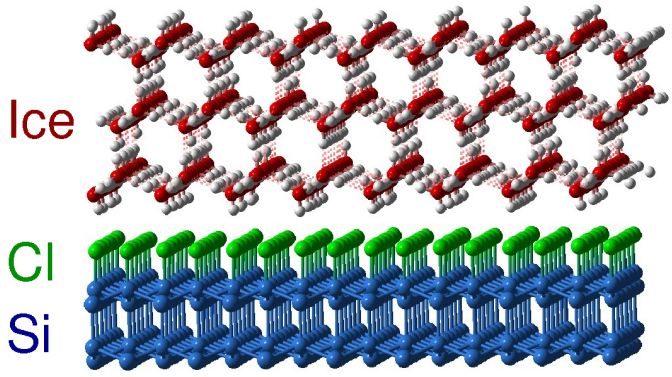

Figure 4.2: Side view of the idealized I_c structure of a three bilayer (3BL) thick interfacial ice on the chlorine terminated Si(111) substrate.

4.2.1 Three bilayers systems

Starting with a proton ordered configuration on a periodic cell (39.90 Å ×30.72 Å ×50.00 Å), classical dynamics simulations have been preformed. Upon slowly heating, the configuration starts to change, still remaining in contact with the substrate. Already at very low temperature (10 K) strong reorganization occurs, with water molecules inverting their orientations; the process is concerted and propagates quickly along the direction normal to the surface. Upon further heating, islands of amorphous ice start to grow on the substrate and the crystal became completely amorphous at about 180 K.

In contrast with the proton ordered configuration, at 70 K the Monte Carlo generated ice I_c lattice (see Figure 4.2) is stable upon the substrate, since just small deviations from the perfect crystal behavior are shown. The different studied parameters (Figures 4.3 to 4.5) are affected only by the presence of a single defective structure, that forms after $\sim$ 150 ps of the equilibration run and lasts for the rest of the simulation (see Figure 4.6(a)). It is generated at the ice-substrate interface, and is mainly due to a reorganization of the

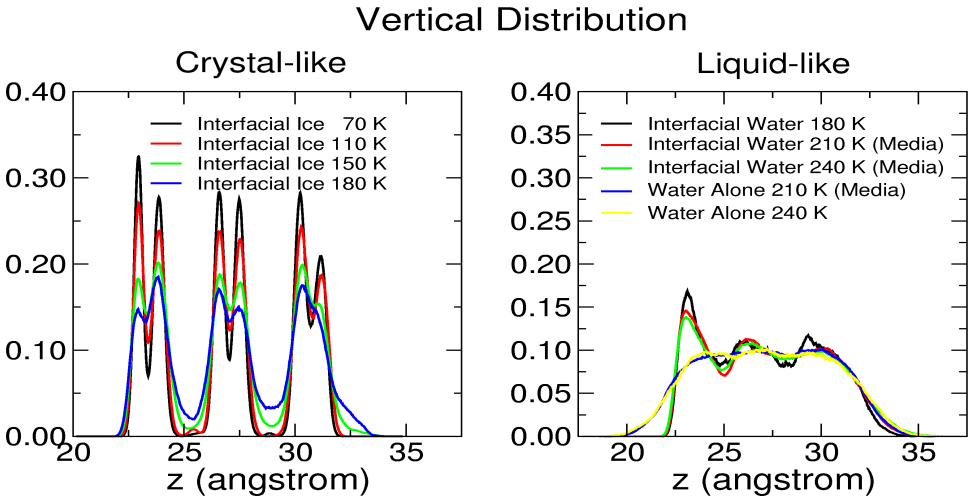

Figure 4.3: Behavior of the distribution function $\rho(z)$ for the 3BL thick system. Left panel: crystal-like structures obtained by equilibrating at different temperatures a Montecarlo generated proton disordered ice I_c configuration. Right panels: liquid-like systems, obtained by melting the crystal structure and by equilibrating at different temperatures the resulting structure. Some of the calculations (Media) were repeated using different random initial velocities and the results were averaged. Calculations are reported also for the system equilibrated in the absence of the substrate (Water Alone).

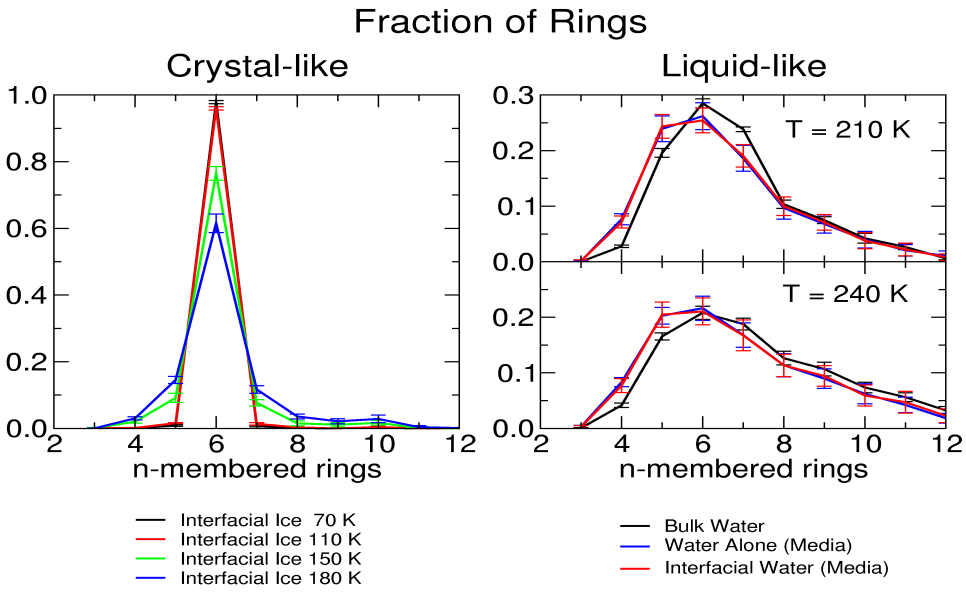

Figure 4.4: Fraction of n-membered rings for the 3BL system. Left panel: crystal-like structures obtained by equilibrating at different temperatures a Montecarlo generated proton disordered ice I_c configuration. Right panels: liquid-like systems, obtained by melting the crystal structure and by equilibrating at different temperatures (top panel T=210 K, bottom panel T=240 K) the resulting structure. Some of the calculations (Media) were repeated using different random initial velocities and the results were averaged. Calculations are reported also for the system equilibrated in the absence of the substrate (Water Alone) and for a box of 1120 water molecules (Bulk Water).

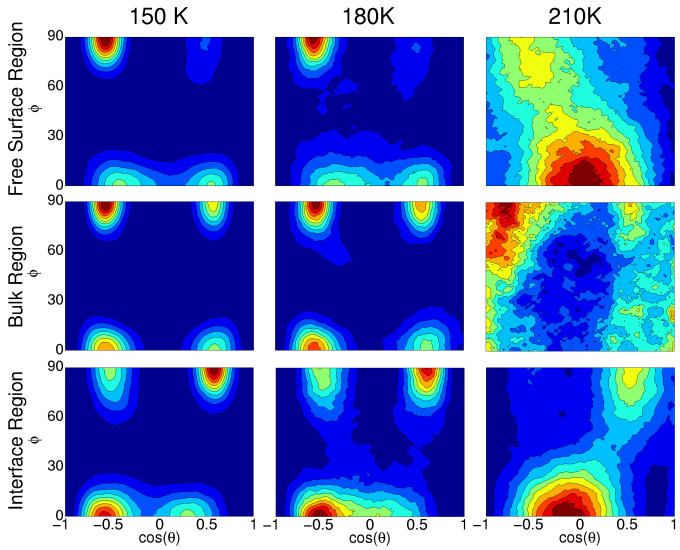

Figure 4.5: Orientational probability distribution $P(\cos\theta, \varphi)$ for the three regions of the 3BL thick interfacial ice. The two independent orientational parameters (θ,φ) are the angular polar coordinates of the vector normal to the substrate's surface (see Figure 4.1) [74]. The presence of four preferred orientations is evident for the crystalline system (below 180 K). At higher temperatures systems present orientational disorder in the bulk region, while molecules at the free surface tend to point towards the inner layers and a more structured bilayer is present at the ice-substrate interface.

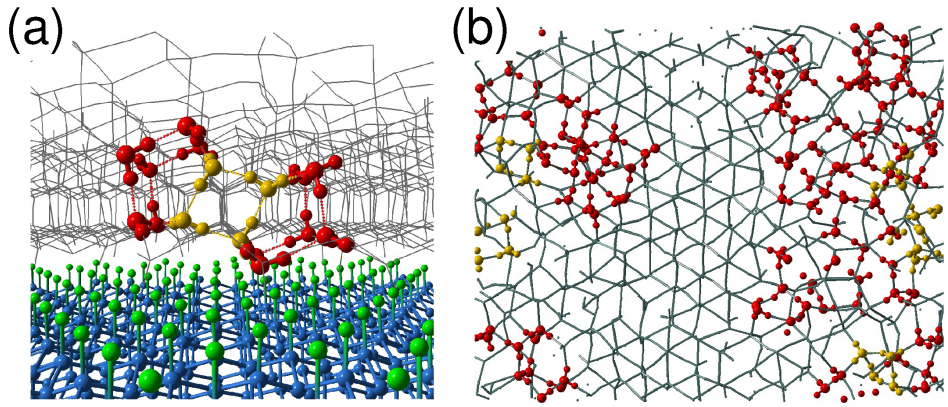

Figure 4.6: Structures of interfacial ice on the chlorine terminated Si(111) substrate: (a) perspective view of a topological defect (a four-membered ring embedded in four five-membered rings) in the interfacial ice equilibrated at 70 K; (b) top view of a 3BL thick interfacial ice configuration equilibrated at 180 K: extended amorphous regions coexist with I_c crystalline domains. The topological reorganization of the interfacial ice is highlighted by depicting water molecules belonging to different n-membered rings in red ($n = 5$) and yellow ($n = 4$), while grey lines represent the defect-free ice structure.

dangling hydrogen bonds pointing toward the interface. The origin of this rearrangement, illustrated in Figure 4.7, arises form the fact that in the ideal 30° rotated interface the water molecule overhanging the interstitial sites of the Cl layer can form only three H-bonds. In order to lower the energy, the undercoordinated molecules lifts and leads to a new bonding pattern where 4-fold and 5-fold rings are formed. This apparently massive rebonding is however obtained via a small but coordinated displacement of the molecules involved. In so doing an extra H-bond is gained. Whether this is a local effects or this mechanism leads to a full fledged reconstruction of the interface it remains to be seen. The presence of the same defect has been observed on both the interfaces also in other simulations at higher temperatures.

Heating the system at 110 K, lead to a small increase of the disorder in the ice

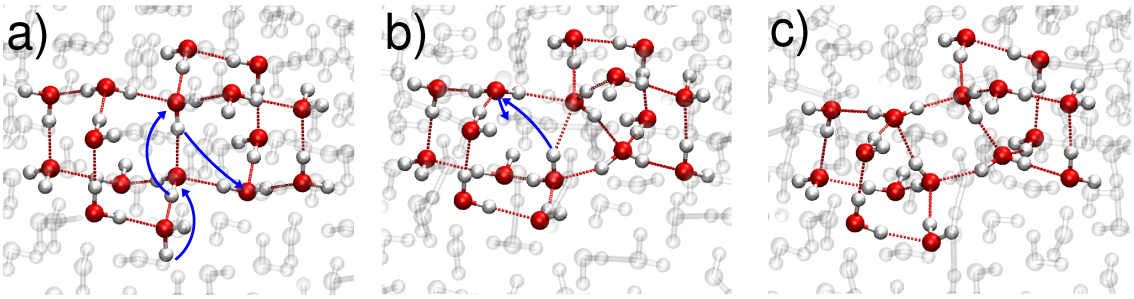

Figure 4.7: Formation of a topological defect at the interface: in the ideal interfacial ice I_c structure (a) some water molecules have a hydrogen atom pointing towards the interface and not participating in any H-bond. In order to maximize the number of H-bonds, one interfacial molecule reorients causing a sudden switch of H-bonds (a). As a result of the rebonding mechanism, a three membered ring is formed together with two five membered rings (b). The internal strain of the network forces adjacent molecules to come closer (b). In order to relax the internal strain the three-membered ring breaks (b), and a stable defective structure composed by a four membered ring and four five-membered rings is formed (c).

network, as evidenced by the broadening of the peaks of the distribution functions. The defective structure formed at 70 K still remains for all the simulation time, during both the equilibration and the NVE simulations.

By equilibrating the system at 150 K, the crystal like structure still persists but small reorganizations occur. Islands of amorphous ice start to grow in different regions of the interfacial film and the partial loss of translational order is evidenced from the loss of features in the radial distribution function and from the different rings statistic.

At 180 K the system approach a phase transition, the regions of amorphous ice increase with respect to the ordered structure, but still the 3BL structure and the orientational order persist (see Figure 4.6(b)).The amount and the distribution of disorder depend significantly on the starting configuration, since different simulations lead to different values of the order parameters. In particular, two configurations presents radial correlation functions broader than the others, and a strong decrease of the number of six-membered

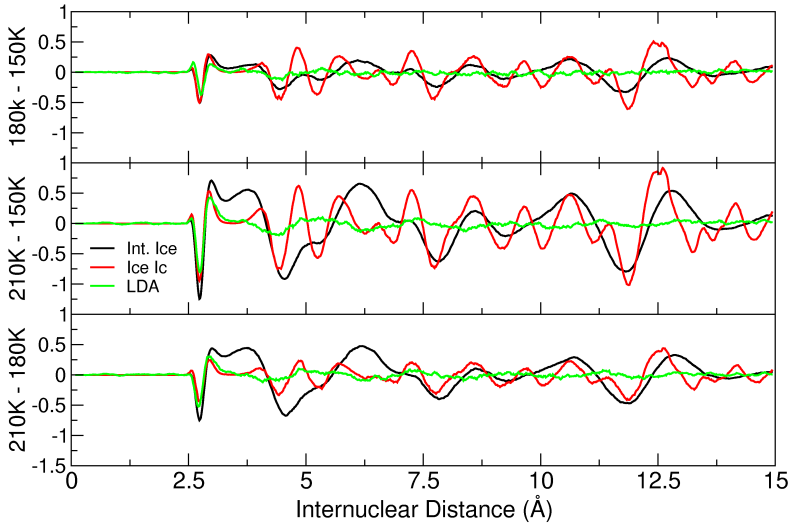

Figure 4.8: Difference radial distribution curves for the three bilayer interfacial ice (Int. Ice, black line) equilibrated at different temperatures (top panel $g\,(r, 180\text{ K}) - g\,(r, 150\text{ K})$; middle panel $g\,(r, 210\text{ K}) - g\,(r, 150\text{ K})$; bottom panel $g\,(r, 210\text{ K}) - g\,(r, 180\text{ K})$). Results obtained for bulk cubic ice (Ice I_c, red line) and low-density amorphous ice (LDA, green line) are also reported.

rings is observed for the same systems (data not reported).

The complete amourphization of the system takes place at 210 K, as evidenced by the loss of structure in the distribution functions. Still, partial orientational and translational order is present for the water molecules close to the substrate, as pointed out from the behaviors of the $P(\cos\theta, \phi)$ and the $\rho(z)$ at 210 K and 240 K (see Figures 4.5 and 4.3). Finally, besides the increased mobility of the system, also the rings statistic of the interfacial systems shows different behavior with respect to that of bulk water (see Figure 4.4). In particular, an increase of the fractions of small rings (four- and five-membered rings) is observed, together with a decrease of the fraction of seven-membered rings. Since the same effect is present in the systems with two free surfaces, it should depend only on the presence of two close interfaces, regardless of the presence of the substrate.

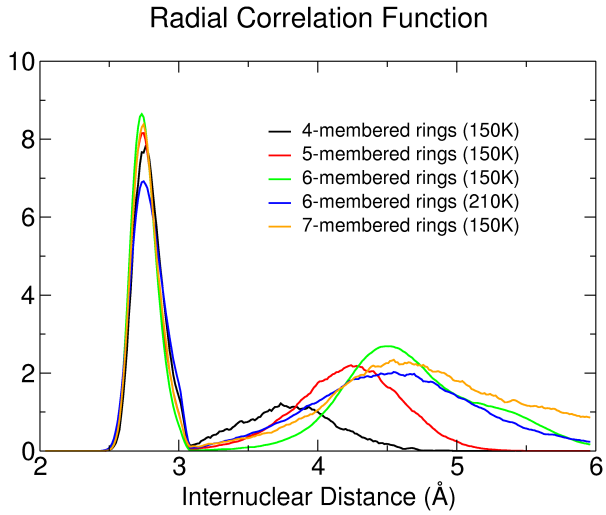

Figure 4.9: Radial distribution function (RDF) of oxygen atoms belonging to n-membered rings (n=4-7) are shown for the system equilibrated at 150 K. The six-membered ring restricted RDF for the system equilibrated at 210 K is also shown to elucidate the thermal effect.

The peculiar disordering process described above, that takes place between 70K and 210K, leads to the g(r) temperature dependence illustrated in Figure 4.8, where a Debye-Waller broadening is superimposed to the increase of configurational disorder. This behavior is similar to the one observed in Ref. [9] during the ultra fast melting process and is characteristic of the thin-layer geometry considered. By comparing the reported temperature dependence with the ones of bulk cubic ice (Ic) and Low Density Amorphous ice (LDA) (also illustrated in Figure 4.8), it is to be seen that interfacial ice at short distances has extra features. In our opinion these extra features are due to the presence in interfacial ice of 4− and 5−membered rings which lead to internuclear distances in the same range. This can be seen from Figure 4.9 where we analyze the pair correlation of water molecules that belong to the same kind of rings.

A separate analysis has to be done for the translational mobility of the system.

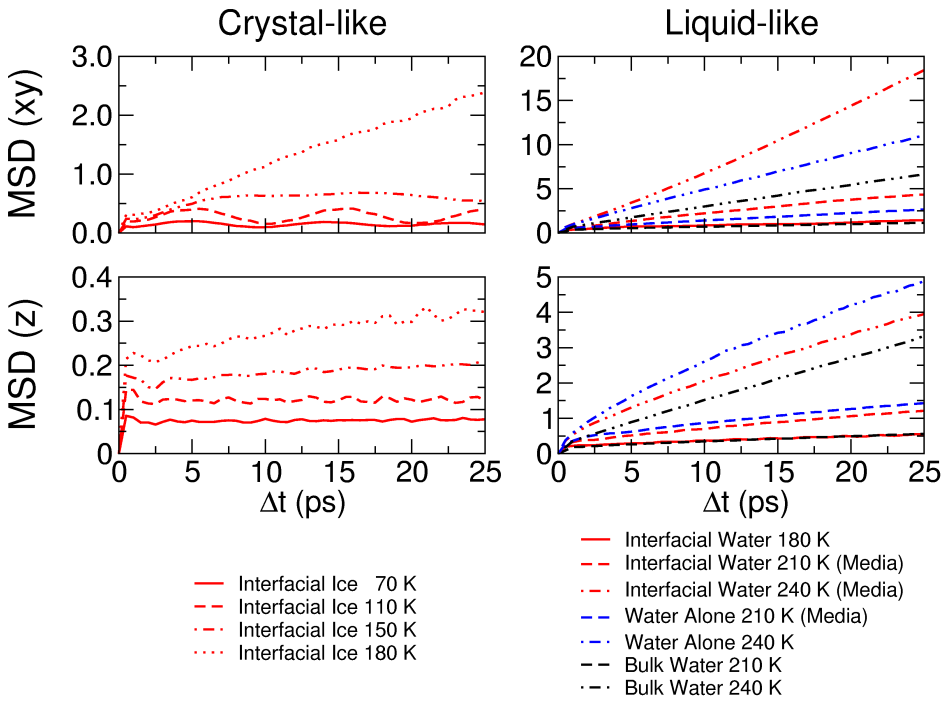

Figure 4.10: Mean Square Displacement (MSD) along the plane parallel (xy, top panels) and perpendicular (z, bottom panels) to the interface for the 3BL thick system. Left panel: crystal-like structures obtained by equilibrating at different temperatures a Montecarlo generated proton disordered ice I_c configuration. Right panels: liquid-like systems, obtained by melting the crystal structure and by equilibrating at different temperatures the resulting structure. Some of the calculations (Media) were repeated using different random initial velocities and the results were averaged. Calculations are reported also for the system equilibrated in the absence of the substrate (Water Alone) and for a box of 1120 water molecules (Bulk Water).

Since no significant differences are present between the three bilayers of ice, only the mean result for D^{xy} and D^{z} have been reported in Figure 4.10. Above 180 K peculiar features appear in the mean square displacement of water molecules, with some of the system analyzed presenting finite and large diffusion coefficients. Since no correlation between diffusion and translational/orientational order is found for these systems, this effect can not be explained in terms of a pre-melting of the the ice structure. In fact, the high increase of the MSD is due to sudden collective movements of the whole ice film along the plane parallel to the interface: the MSD along this directions is bigger than the ones calculated for the same systems but without the substrate (see top panels of Figure 4.10). These collective moves tend to optimize the match between the ice lattice and the substrate and do not depend on the equilibration time of the system, since they occurs at random times also in longer simulations. Since in our calculations the substrate was let free to move, calculations have been repeated fixing few positions of the silicon atoms, in order to see if this lattice matching effect was due to an artifact of the simulations. Nonetheless, diffusion coefficient similar to the previous ones were found and the collective moves were still present in the repeated calculations. Because of this effect, only the component of the MSD perpendicular to the substrate (z-axis) can be used to evaluate the translational mobility of the water system.

As the system temperature increases above 210 K a liquid-like behavior was found characterized by a finite diffusion coefficient. Nonetheless, also simulating a totally amorphous configuration of the interfacial ice at 180 K, a liquid-like behavior was found, with a diffusion coefficient along z similar to the one of undercooled bulk water at 210 K. This

liquid-like interfacial water shows an increased mobility with respect to bulk water also at higher temperatures. This effect was already found in other interfacial systems and can be explained in terms of the increased number of degrees of freedom for the molecules close to the free interface. For this reason, the same effect is even stronger for the water film without the substrate, in which two free interfaces are presents (see bottom panels of Figure 4.10).

Metadynamics

Since the Monte Carlo generated configurations are stable on a wide range of temperatures, a metadynamics study of the free energy of the system is possible, starting from a crystal-like structure. The method [82–86] is based on a coarse grained history dependent potential approach in extended Lagrangian framework and relies upon the choice of a set of collective variables that can be any function of the atomic positions. Then, an extended Lagrangian MD is run, where an additional variable for each collective variable is added. The additional variables feel the effect of the previous history of the run by means of a Gaussian repulsive potential. For this fictitious dynamics to be effective the chosen collective variables should be able to properly describe the reaction coordinate, being capable, at the same time, of discerning between initial and final states of the reaction. Moreover, in the collective variables space all of the reaction modes having similar characteristic times should be included.

The order parameters used in this simulations are the Q_6 and the $S\left(\vec{k}\right)$, with $\vec{k}$ corresponding to the (220) ice Ic reciprocal lattice in order to characterize the long range translational order along one of the direction parallel to the interface. The temperature of the simulation was 120 K to avoid a too fast scanning of the ordered initial configurations.

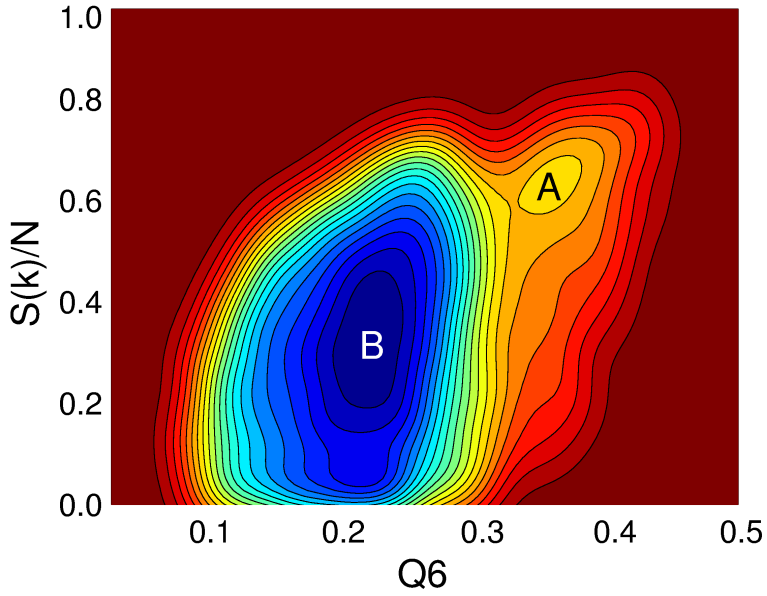

Figure 4.11: Free energy surface reconstructed using metadynamics with the Q_6 order parameter and the normalized structure factor $S(\vec{k})$, with $\vec{k}$ corresponding to the (220) ice I_c reciprocal lattice vector. Two main basins were reconstructed, corresponding to the ideal crystal configurations (A) and to partially disordered structures (B).

Nonetheless, the free energy surface so reconstructed is incomplete due to the slow diffusion time of the system in the phase space of the collective variables adopted. In particular, at the considered temperature the simulation never visited the region of completely amorphous structures. In fact, from a 2ns long simulation of the system, two main basins are evident, corresponding to the ideal crystal configuration and to partially disordered structures (respectively region A and B in Figure 4.11). The latter is the most stable state reached by the system already at the low temperature considered.

4.2.2 Nine bilayers systems

Increasing the thickness of the interfacial ice lead to an increase of the system stability. By equilibrating the system at increasing temperatures, reorganization at the

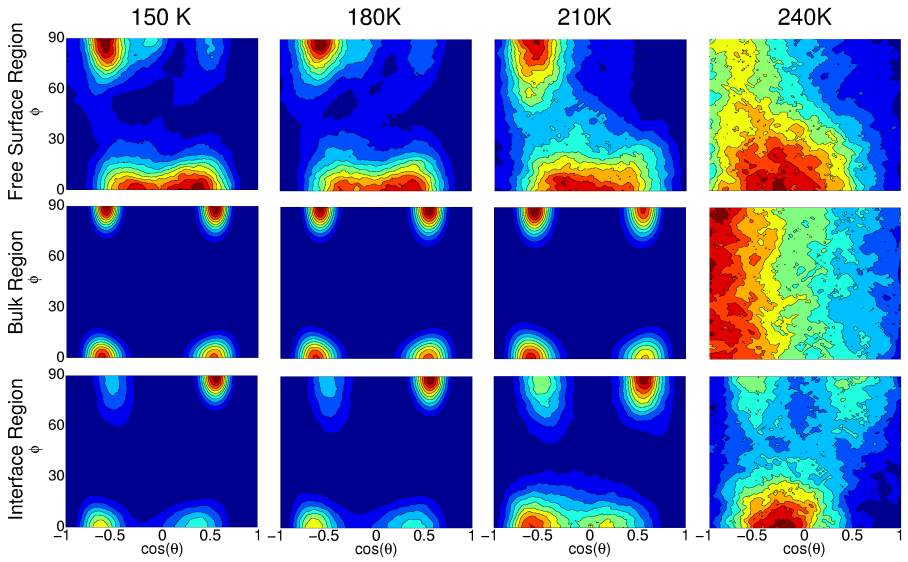

Figure 4.12: Orientational probability distribution $P(\cos\theta, \varphi)$ for the three regions of the 9BL thick interfacial ice. The presence of four preferred orientations is evident for the crystal-like systems (below ∼210 K). Once melted (240K), the system presents completely azimutal (φ angle) disorder in the bulk region, but a preferred orientation of the water dipoles towards the substrate is found. Molecules at the free surface points preferably towards the inner layer while a more structured bilayer is present at the ice-substrate interface.

two interfaces occurs, but the inner bulk region is less affected and remains substantially crystalline until the TIP4P melting temperature is reached.

Apart from the bulk region, the considerations done for the two interfaces in the 3BL systems still hold for the 9BL ice. Since the lattice matching effect is still present in the thicker system, only the diffusion coefficient along z has been reported. Nonetheless, in this case the contributions arising from the different layers have been analyzed (see Figure 4.14).

As shown in the $P(\cos\theta, \phi)$ and $\rho(z)$ plots (Figures 4.12 and 4.13), the ice network at the free surface reorganize already at low temperature (150 K) in order to reorient the water molecules towards the inner layers. The mobility of this water molecules is greater

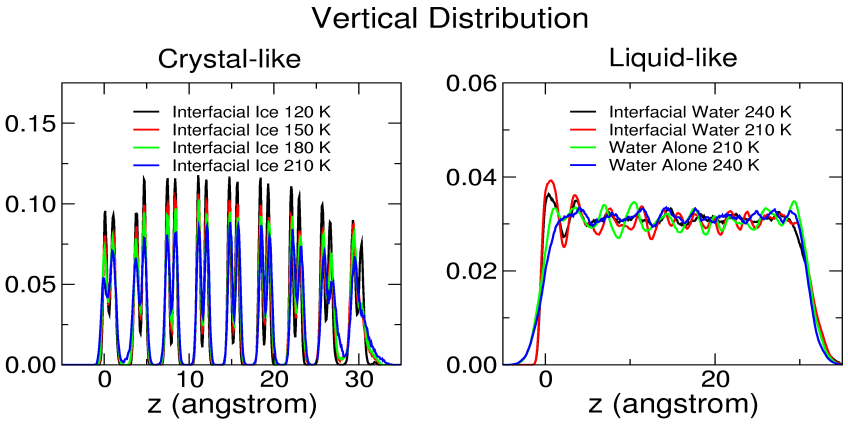

Figure 4.13: Behavior of the distribution function $\rho(z)$ for the 9BL thick system. Left panel: crystal-like structures obtained by equilibrating at different temperatures a Montecarlo generated proton disordered ice I_c configuration. Right panels: liquid-like systems, obtained by melting the crystal structure and by equilibrating at different temperatures the resulting structure. Calculations are reported also for the system equilibrated in the absence of the substrate (Water Alone).

than for the rest of the system and it is also greater than the corresponding mobility of bulk water. Also in this case the effect is due to the increased number of degrees of freedom. The number of ice molecules affected by this reorganization increase by heating the system and it goes from the topmost bilayer at 120 K to one-two bilayers at 150 K-180 K and to two-three at 210 K.

As for the water-substrate interface, the ice network disruption followed by the formation of defects and amorphous regions is also observed. This effect is different from the previously analyzed reorganization, since it involves a smaller region of the crystal (almost only the first bilayer for simulations below the melting temperature) and the diffusion coefficient of the water molecules is not liquid-like (see Figure 4.14). In fact, there is a decrease on the number of degrees of freedom with respect to bulk water, since water molecules can not penetrate inside the surface. In addition, water molecule at the interface

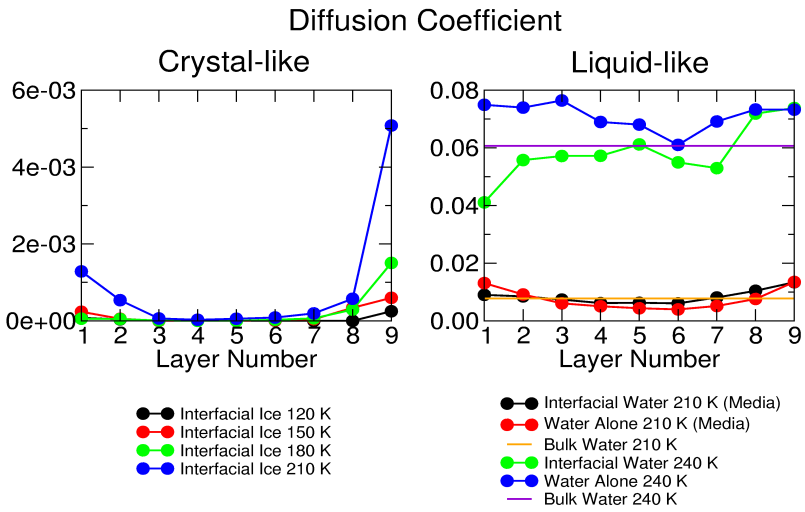

Figure 4.14: Diffusion coefficient (Å^2/ps) along the direction perpendicular to the interface (z) for the different layers of the 9BL thick system. Left panel: crystal like structures obtained by equilibrating at the different temperatures the Montecarlo generated proton disordered ice I_c configurations. Right panels: liquid-like systems, obtained by melting the crystal structure and by equilibrating at different temperatures the resulting structure. Some of the calculations (Media) were repeated using different random initial velocities and the results were averaged. Calculations are reported also for the system equilibrated in the absence of the substrate (Water Alone) and for a box of 1120 water molecules (Bulk Water).

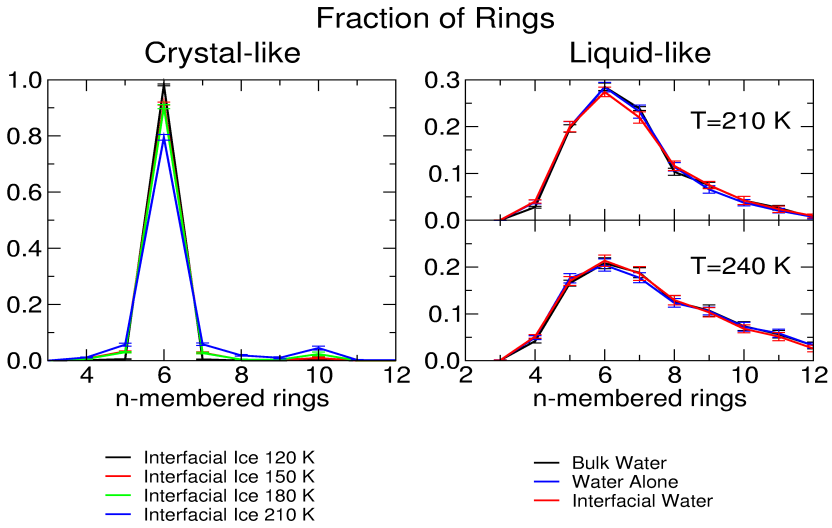

Figure 4.15: Fraction of n-membered rings for the 9BL system. Left panel: crystal-like structures obtained by equilibrating at different temperatures a Montecarlo generated proton disordered ice I_c configuration. Right panels: liquid-like systems, obtained by melting the crystal structure and by equilibrating at different temperatures (top panel T=210 K, bottom panel T=240 K) the resulting structure. Some of the calculations (Media) were repeated using different random initial velocities and the results were averaged. Calculations are reported also for the system equilibrated in the absence of the substrate (Water Alone) and for a box of 1120 water molecules (Bulk Water).

tends to reorient their dipoles towards the substrate surface, and not to the inner most layers. Thus, electrostatic effects are responsible for the observed amourphization of the ice-substrate interface.

As pointed out for the 3BL system, the presence of the two interfaces give rise to a small increase in the number of four-membered rings with respect to bulk water (Figure 4.15). Nonetheless, due to the increase of the non-interfacial region in the thicker system, this effect is less pronounced and no significant deviations from the bulk water behavior can be found in the statistic of rings of bigger dimension.

At 240 K, the thickness of both the two interfacial layers slowly increases and the

complete melting of the crystal is observed after a 1.5 ns equilibration run. Still, electrostatic effects play a role in reorienting water molecules, as evidenced from the structured first bilayer, from the reduced mobility of the interfacial region and from the net orientation towards the substrate of water molecules belonging to the bulk region (Figures 4.14 and 4.12).

4.3 Crystallization

In order to further asses the validity of the studied configurations of the interfacial ice, few attempts have been made to crystallize bulk water on top of the substrate. Water crystallization is known to be a slow process [87], but in the presence of an electric field o in supercooled systems the characteristic timescale can be substantially lowered [72, 73]. Nonetheless, trying to anneal the liquid water upon the considered substrate, lowering the temperature from 240 K to 180 K, bring the system to completely amorphous ice and not to a long-range ordered phase. For the considered simulation times (up to 3.0 ns), the potential induced by the surface is not strong enough to overcame the kinetic barrier for crystallization to happen.

4.3.1 Metadynamics

A possibility is to use metadynamics to overcome free energy barrier and thus simulating the rare event we are interested in. In fact, the methodology has been successfully used to simulate bulk melting [76] and to speed up phase transitions in condensed matter [88,89]. Few combinations of the Q_6 order parameter and the $S\left(\vec{k}\right)$ for different wavevectors

have been tested, but in all cases simulations have not succeeded to bring the system into the crystal phase. The free energy surface in the multidimensional space of the collective variables was reconstructed too slowly and in fact not all the slow degrees of freedom were included in the definition of the collective variables: the results is that even if the collective variables reach the correct values, the corresponding configuration is not the crystalline one, but it is a metastable state that immediately goes back to the amorphous if it is left free to equilibrate.

Chapter 5

Non-equilibrium dynamics

5.1 Simulating laser heating and heat diffusion

In order to simulate the experimental conditions, few attempts have been made to characterize heat diffusion inside the system. We have tried to solve the equation for a monodimensional system both numerically and analytically, but we missed from the experiments some of the initial conditions (in particular, informations on the temperature profile after the temperature jump were missing). Thus, our approach has been to make reasonable assumptions and compare the results with the experimental outcome. We report here only one set of simulation which better reproduces the experimental results, but within the uncertainty of our calculation they all give coherent results.

The starting system was the 9BL thick interfacial ice analyzed in the previous section with fixed position of one of the silicon atoms, in order to avoid collective movements of the substrate. Since it is well known that the melting point of TIP4P water is 15% lower than that of real water [64, 65], simulation have been performed starting from the system

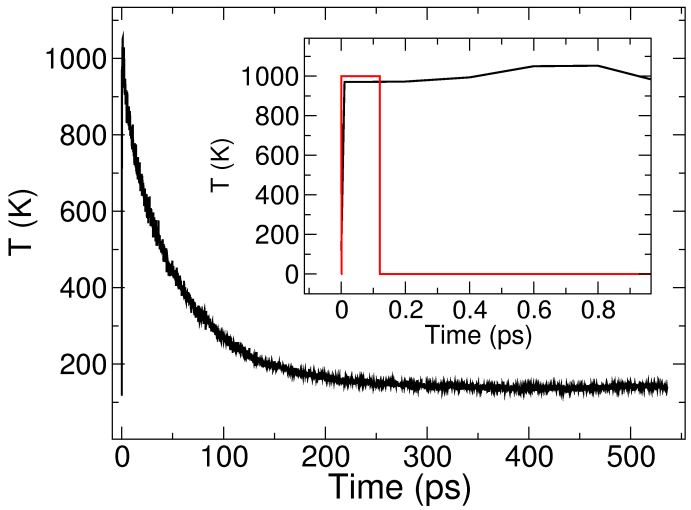

Figure 5.1: Behavior of the temperature (black curve) of the substrate during an example of the simulation of the experiment. The system is equilibrated at 120 K before the beginning of the simulation. In order to simulate laser eating the Si atoms kinetic energy is brought to the value corresponding to a fixed target temperature, in the example $T^{pulse} = 1000$ K (red curve in the inset), for a duration corresponding to the experimental duration of the laser pulse (120 fs). After having turned off the pulse, a thermostat was applied to the system to simulate heat dissipation.

equilibrated at 120 K, which is lower than the experiment.

In order to simulate the effect of laser heating the Si atoms kinetic energy is brought to the a value corresponding to a target temperature T^{pulse}. This is obtained by rescaling at every time step the Si velocity for the duration of 120 fs, which is the laser pulse duration. After having turned off the pulse we let the system relax toward equilibrium (see Figure 5.1). Due to the small system size we can simulate heath dissipation only by applying a thermostat. We have chosen to use a Berendsen thermostat which has an arbitrary characteristic relaxation time τ. Simulations were performed using different values of these two parameters, T^{pulse} ranging between 300 K and 2000 K while τ ranging between 5 ps and 100 ps, in order to monitor their effects on the final outcome.

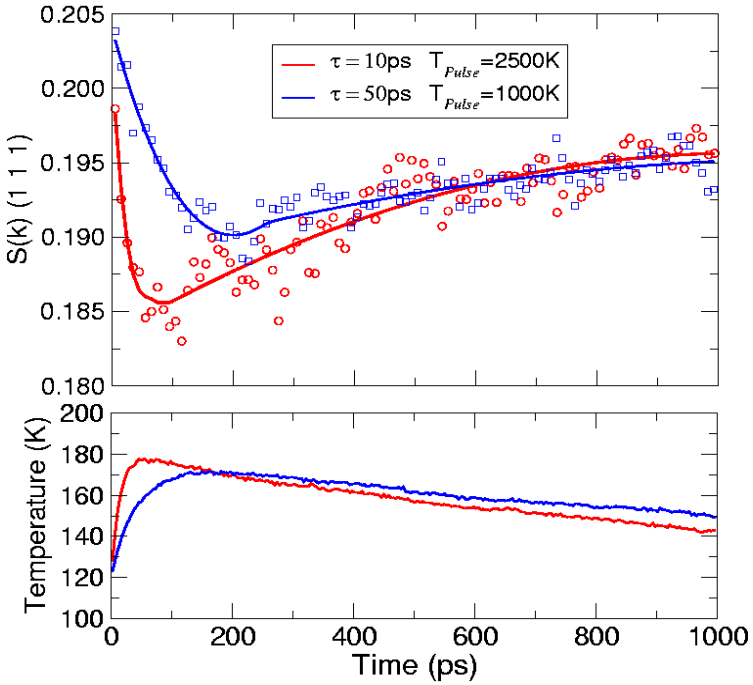

Figure 5.2: Top panel: time evolution of the normalized structure factor $S(k)$ for the (111) vector of the ice I_c reciprocal lattice. Two choices for the relaxation time are given: $\tau = 10$ ps, $T^{pulse} = 2500$ K (blue curves) and $\tau = 50$ ps, $T^{pulse} = 1000$ K (red curves). Bottom panel: instantaneous temperature of the water molecules during the non-equilibrium dynamics.

5.2 Results

In Figure 5.2 the results that best reproduce the qualitative outcome of the experiments are reported. In particular, the choices of the parameters that best reproduce the experimental behaviors are the ones with $T^{pulse} = 2500\,\mathrm{K}$ $\tau = 10\,\mathrm{ps}$. In both cases, the behavior of the (111) $S(\vec{k})$ peak has a minimum at time slightly delayed relative to the temperature maximum and on the time scale of the experiment the initial order is not recovered. More striking is a direct comparison with the diffraction data in Ref. [9] (Fig. 3I). The simulated time evolution of the (111) diffraction peak (Figure 5.3) displays the

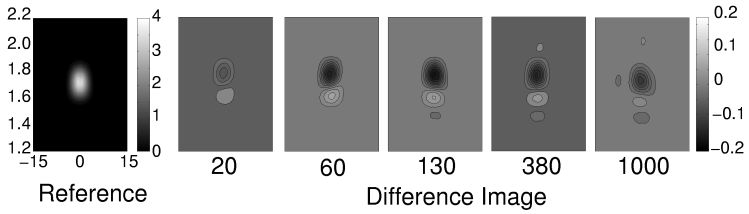

Figure 5.3: Diffraction difference images for the (111) Bragg spot at different times (ps), for the $\tau = 50$ ps, $T^{pulse} = 1000$ K simulation. The vertical axis is the momentum transfer coordinate (Å^{-1}) and the horizontal axis is the azimuthal scattering angle (°).

same features of the experiments, namely a depletion region at about $1.8\,\text{Å}^{-1}$, which is compensated by an increase of the signal around $1.6\,\text{Å}^{-1}$. We also observe that at the end of the simulation ($t = 1\,\text{ns}$) the difference image is attenuated. Examining the MD trajectory and from the analysis of the $S(\vec{k})$ for the different regions, we relate the behavior of the diffraction signal to thermal broadening and to a reorganization of the ice-vacuum interface layers. In particular two different processes seem to concur to the decrease of the structure factor: first, the instantaneous breakage of isolated hydrogen bonds, mainly along the direction perpendicular to the surface; second, the creation of topological defects, mainly at the interfaces. Evidences of these behaviors come from the analysis of the ring distribution along the trajectories (Figure 5.4): it is clear that the decrease in the number of six-membered rings is due to the creation of small membered rings (with structure similar to the ones reported previously) and to the creation of ten-membered rings. As already noticed, ten-membered rings are formed when a single hydrogen bond, shared by two otherwise perfect six-membered rings, is broken: thus it accounts for the number of single hydrogen bonds that breaks along the simulation. Moreover, from the analysis of the structure factor behavior, it comes out that the breakage of six-membered rings is mainly

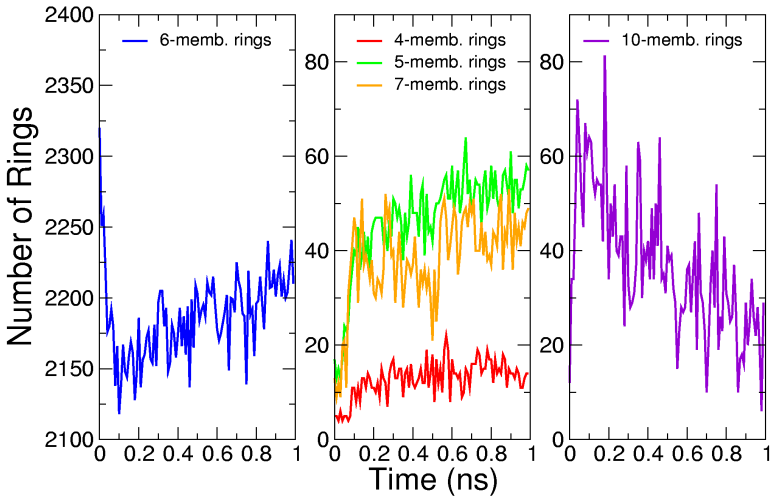

Figure 5.4: Behaviors of the number of n-membered rings along the duration of the simulated experiments. The system, composed mainly of six-membered rings (left panel), loose part of is topological order as the heat dissipate from the substrate through the interfacial ice. Part of the ice network reorganize and form topological defects composed mainly of small membered rings (4- and 5-membered rings, central panel). These defects persists until the end of the experiments. Reorganization of the network occur also through the elongation and breakage of single hydrogen bonds in an otherwise ideal ice structure: this process is well described by the number of ten-membered rings (right panel) and is almost reversible within the timescale of the simulations.

due to an elongation of the ice network along the 111 direction. The relative intensity and speed of these two processes, depend on the parameters of the simulation, but while the former is substantially reversible (as shown by the complete recovery of the original number of ten-membered rings in Figure 5.4), the second is irreversible on the timescale of the simulation (as shown by the number of five and four membered rings in Figure 5.4).

Part II

Structure of a water overlayer at the Pt(111) surface

Chapter 6

Introduction

6.1 Interfacial water

The structure of water at the interface with other materials determines their wetting properties and underlies the vast array of phenomena known under the names of hydrophobicity and hydrophilicity. These phenomena are crucial in biology and in material sciences. It is therefore not surprising that the study of interfacial water structure is a subject of great interest. Indeed, numerous studies are devoted to this subject and different reviews concerning this subject appeared in the literature in the past years. The first one, compiled by Thiel and Madey in 1987 [1], describes more than two decades of experimental and theoretical studies. After less than fifteen years the need for a second review on the subject emerged, and brought to the appearance in 2002 of the Henderson's review [2]. More recently, in 2005 an entire issue of Current Opinion in Solid State and Materials Science was devoted to the subject of water at interfaces [90, 91] and in 2006 the same happened with the Chemical Review journal [3, 4]. The number of reviews together with the shortening of

the time interval between different reviews are clear evidences of the increasing interest and of the accumulation of new results.

Theoretically, the problem of water adsorption on a substrate and the characterization of the structure of water overlayers received much attention since the beginning of computer simulations. Systems were first investigated by means of *ab-initio* (mainly Hartree Fock) calculations on small clusters. Calculations using the Density Functional Theory on periodic systems followed. Most of the studies in the literature present single point energies calculations and geometry optimizations. Despite the dimension and the complexity of the systems under investigation, also *ab-initio* Molecular Dynamics (MD) calculations have been recently reported. Classical MD simulations have been used to describe systems characterized by higher thickness of the water film and to model amorphous and liquid overlayer. Nonetheless, due to the poor quality of the available classical force fields in describing the substrate-water interaction, most of the classical MD calculations failed to reproduce the basic features of the systems under investigation (see for example the case of platinum in Section 7.2.3).

Experiments on water adsorption require the use of surface sensitive techniques: while in recent years different works using scanning probe methods appeared in the literature, the most used experimental techniques include core level spectroscopy (like XPS, XAS and XES) as well as IRAS, Raman and sum frequency generation. Crystallographic techniques such as LEED, are also widely exploited, while Thermal Desorption Spectroscopy is most used in system characterized by higher thicknesses of the water film.

6.2 Characterization of the problem

The task we are dealing with is the determination of the structure of water adsorbed on top of a substrate. Thus, first of all it is necessary to define the characteristics of the starting system and the quantities/features of the structure we want to determine.

The starting system is characterized mainly by three factors: the **substrate**, the **substrate's surface** and the amount of **water coverage**. In order to join a picture as clear as possible of the involved processes, most of the studies (both experimental and theoretical) deal with 'simplified' systems: in fact the majority of the works that have been reported in the literature regards crystalline interfaces, were the microscopic mechanism of water adsorption could be more easily modeled. In particular, these studies involve transition metals' crystalline surfaces, like the fcc(111) and the hcp(0001) surface. A water coverage ranging from single molecule to one or two layers of molecules has been examined. Molecular scale studies encompassing more than just one or two layers are not abundant, mostly due to limitations in the experimental techniques.

Since the metal is often only slightly affected by the wetting process, the final structure is characterized only in terms of the structure of the water molecules. Moreover, mostly ordered water overlayers are studied, due to the fact that amorphous water adsorption can be less easily modeled. The water structure is characterized by four main aspects: the long-range order (the **kind of reconstruction**), the **heights distribution** of the oxygen atoms, the presence/amount of **dissociation** (reactive wetting) and the presence of **proton order**/disorder. The two former aspects regard mainly the position of oxygen

atoms above the substrate, while the two latter are related mostly to the hydrogen atoms positions.

Reconstruction: it identifies the water molecules lattice and the orientation of the lattice with respect to the underlying substrate's surface. Since the majority of the studied substrates' surfaces exhibits hexagonal periodicity, the same long range order appears in most of the water lattices. Depending on the lattice mismatch between the metal and the water lattices, the latter can and usually are tilted with respect to the former. The easiest reconstruction is obtained for most of the metal substrates with a tilting angle of 30 degrees. Some times, more complex structures have been reported, in which different lattices coexist on the same substrate or in which structures with lower periodicity (water rods and water islands) form.

Height distribution: apart from the distribution of the water molecules along the plane parallel to the interface, also the vertical distribution of the oxygen atoms can be strongly modified by the substrate. This aspect is important both theoretically, since it is a direct consequence of the metal-water interaction, and experimentally, since many techniques can give a direct estimate of such a distribution. Usually one distinguish between flat water monolayers and puckered water bilayers. In some cases, the bimodal character of the height distribution was found to be extremely pronounced, with some water molecules at short metal-oxygen distances connected with water molecules far away from the substrate (see for example Chapter 8).

Dissociation: depending on the relative affinity between the metal surface and the oxygen atoms, reactive wetting may occur. The general result of such a process is the dissociation of a water molecule with the formation of a metal-OH bond. It is not possible to identify the final position of the dissociated hydrogen atoms due to the high mobility of such particles and to the experimental difficulties of determining hydrogen positions. Depending on many factor, like the system preparation route, similar systems can be characterized by different degrees of dissociation: in some cases, e.g. for platinum, the structure composed by a 1:1 ratio between dissociated and undissociated species was found to be the most stable. Nonetheless, even if the chosen substrate does not promotes water dissociation, it can stabilize the product of water self-dissociation and a substantial fraction of dissociated species can be found close to the interface.

Proton order: finally, to characterize the structure of the water overlayer it is necessary to identify the kind and degree of proton order, i.e. the position of the hydrogen atoms with respect to the oxygen network and to the substrate. The latter aspect is the most discussed in the literature in relation to the structure of the first water layer. A general distinction in H_{down} and H_{up} structures is done in the literature, depending whether water molecules at the interface prefer to orient their hydrogen atoms toward the substrate or not. Such out of plane proton order can have macroscopic effects on the system leading to a net dipole moment that in principle can be measured. Nonetheless, for thick and large systems the overall effect is predicted to be negligible, since proton disorder is entropically favoured in most of the water structures. The existence and stability of more disordered structures, so called H_{mix} structures, characterized by a zero out of plane net dipole of

the water system, were predicted theoretically. As for the in-plane proton order, very few studies have dealt with such an effect. Nonetheless it is possible that proton order stabilizes the water structure and, in particular, proton ordered structures were proposed for partially dissociated overlayers.

When considering these different aspects, one of the most common approximation is to assume that each one of those is independent from the others. In doing so, it is possible to focus on a specific feature of the system. Of course such an approximation can give reasonable results only if the energies involved in each of the different aspects are very different or if there are external factors that fix one of the aspects. In general for most of the systems studied this is NOT the case. The *quantity* and the *quality* of each one of these factors have an influence on each other.

6.3 General results for metals

One of the aims of the theoretical analysis of these problems is to explain the formation of one structure in term of simple physical aspects of the system. In particular the main ingredients that enter the problem are the strength of the metal-water bond and its spatial dependence together with the strength of the metal-hydroxyl bond and its spatial dependence. This two quantities have to be compared with the strength and directionality of the water-water bond, that is a well known and studied problem.

To get a reasonable estimate of the relative strength of these different aspects, the first step is the study of the adsorption of water monomers.

General results for water monomers adsorption: the energetics of adsorption of water monomers on different (111) metal surfaces have been studied theoretically in several articles [92–96]. Using density functional theory, Michaelides et al. found that, in general, the favored adsorption site of the monomer is on top of the metal atoms, were the O lone pair orbital hybridizes with the metal orbitals to form a covalent bond [94]. In particular the bond with substrate is mainly due to the interaction of the unoccupied 5d states of Pt atoms with the $1b_1$ occupied molecular state of water. The optimal geometry is the one where the plane of the water molecule lays nearly parallel to the surface. The adsorption energies were found to vary from 0.1 to 0.4 eV, which is of the order of magnitude of the energy of a hydrogen bond (~ 0.25 eV). The adsorption energy depends on the metal and was found to be ranked in the order Au < Ag < Cu < Pd < Pt < Ru < Rh which reflects the strength of the oxygen-metal bond. The differences in binding energies upon slight displacement of the water molecule and slight rotation were found to be as low as 0.02 eV. This lead to the suggestion that adsorbed water will be randomly oriented on the surface at temperatures above few degrees Kelvin. Moreover, the weak dependence of the binding energy on these two parameters implies that monomer in adjacent sites can easily reorient to form dimers. The energy gain associated to the formation of hydrogen bond can, in those cases, overcome the loss in energy due to the unfavorable position and orientation. As a consequence, it is common to find structures with small lattice mismatch and different water orientations.

Following these findings, many studies than focused their attention to the extended systems. Indeed, as the water coverage on the surface increases, monomers form clusters

that eventually merge in extended structures. The formation of chains and monolayers was reported for several metals [97, 98] and many studies focus on the creation of full monolayers [99–101]. The main idea is that, depending on the relative strength of the water-water interaction in a layer and across layers, water will wet or not the surface. In the former case the structure of the system is characterized by the presence of flat multilayers, while in the latter case the formation of three dimensional islands is observed.

The Doering and Madey model: the simplest way to take into account the above described properties in the case of a non-dissociated monolayer is the model proposed by Doering and Madey in1982. According to this model the water monolayer adopts the structure of the puckered honeycomb found in the basal plane of ice I_h [102]. Water molecules at the interface are adsorbed at atop positions. In this way both the water network and the water-metal interaction can be maximized simultaneously. Indeed, the water layer was found to be in many cases in registry with the surface lattice of fcc(111) and hcp(0001) metals, based in part on LEED observation of a $\left(\sqrt{3} \times \sqrt{3}\right) R30^\circ$ structure. Supported by some experimental results, this model gained popularity and was widely used mostly for its theoretical simplicity. Indeed, its high symmetry allowed the use of relatively small simulation cells in theoretical studies. It had been commonly accepted that hydrogen atoms that are not part of H-bond were pointing up perpendicular to the surface, in what is called the H_{up} configuration.

Nonetheless, the approximation of the physics of the system discussed above lead to an oversimplification of the problem. Following the first works based on the assumption of the ice bilayer model [102], some limitations of this ideal configuration were soon pointed out

in the literature. In order to explain experimental results, other proton configurations were suggested and the possibility of partial dissociated structures (characteristic of a 'reactive wetting' mechanism [101]) was proposed [103]. Starting from this models, DFT calculations were performed to examine the stability of intact layers with alternating molecules in the H_{up} and H_{down} configurations, as well as of half dissociated layers on different metals. The stability of half dissociated layers varies considerably between substrates, whereas the stability of intact monolayers does not. A careful analysis of the different contributions to the total binding energy, separated into those arising from H-bonding inside the layer and those arising from bonding to the metal substrate, was performed to explain this result [104]. The analysis revealed that the largest contribution to the binding energy of the layer was due to the internal H-bonding, while the bonding to the substrate contributes only a 30-20% of the total energy. As to the partially dissociated structure, stability arises from the OH absorption energy which compensate the loss in oxygen-metal binding energy. These Authors report that the results are sensitive to the final positions of hydrogen atoms. Since in this study the minimal $\left(\sqrt{3}\times\sqrt{3}\right)R30^{\circ}$ unit cell with perfect proton order was considered, no systematic search for the lowest energy structure was possible.

Indeed, the use of such strong periodic boundary conditions was shown to not allow the complete relaxation of the water structures. In addition, the possibility of re-arrangements with reduced periodicity was ruled out. In different cases, like for Pt and Ru, this possibly has turned out to be an important factor since experimental evidence indicate that the most stable structures have a larger primitive unit [97, 98, 105].

In most cases, the inclusion of long range and size effects can substantially decrease

the differences between alternative structures. Indeed in large systems many different structures exists, with a stability comparable or greater than the one of the Doering and Madey model. The problem is more pronounced for properties, like proton order, that intrinsically depend on the entropy of the system. Theoretically the complexity of the problem is due to the fact that the difficulty in the search for the minimum energy structure grows exponentially with the systems size. For instance the experimentally observed water on platinum reconstruction, which has 39 water molecules in the unit cell, is probably beyond present day capabilities.

The complexity of the potential energy surface has also important consequences on the outcome of the experiments and their interpretation. For instance local minima can be stabilized either by impurities or by kinetic effects. Furthermore invasive probes, like energetic electrons in LEED experiments, can induce transitions to a different minimum.

Chapter 7

Water on Pt(111)

7.1 Experimental background

7.1.1 General properties of water adsorption

Water molecules attach to the Pt(111) surface at low temperature by forming monomers in flat configurations in atop positions [106, 107]. The low energy barrier for translation and rotation of the water molecule over the metallic substrate allows water molecules in adjacent sites to rearrange and eventually form small clusters at temperatures as high as 40 K. Desorption of single water molecules starts to occur at temperatures above 135 K. Below this temperature, high dose of water adsorption leads to the formation of amorphous solid water (ASW) at the interface [108].

Crystalline ice can be formed by dosing water at $T > 135$ K or by annealing ASW above 150 K, the onset of crystallization being indicated by a drop of the vapor pressure or by change in the IR band shape [105, 109, 110]. The evolution of the crystal structure is

reflected in the uniform grow of the ice features in RAIRS and by the uniform increase in the TDS peaks. At submonolayer coverages the water stitching probability on the substrate is almost unitary. The completion of the first ice layer on the substrate is reflected by a sudden drop in the sticking probability, that eventually becomes zero at temperatures as high as 144.3 K, when the rates of adsorption and desorption of a second layer water become equal. As the film growth continues, no other abrupt changes in the sticking probability have been reported, coherently with a Stranski-Krastanov mechanism to form a three dimensional ice after the first bilayer is complete [110]. Growth of crystals as thick as 150 ML has been reported [111].

The first water layer desorbs molecularly from the metal near 170 K, leaving a clean Pt(111) surface [112–115]. Nonetheless, partial dissociated water overlayers have been characterized in water production reaction [116–121]. The occurrence of water dissociation in the interfacial layer has been also recently reported by experiments on thick ice films at high temperatures ($T > 150$ K) [111]. Whether this effect is temperature induced is still an open question but it is worth to mention that first layer structures containing dissociated species have been theoretically predicted [93, 122, 123].

Starting from the above considerations it is possible to divide the literature about water-Pt systems in three parts: two focusing on the first layer structure, both the intact and the half-dissociated monolayer, and one on multilayer films.

7.1.2 Non dissociated water monolayer

The intact water monolayer has been extensively studied experimentally by means of IRAS, LEED and core level spectroscopies. The evidence of a $\sqrt{3} \times \sqrt{3}R30$ LEED

pattern [124] was used to validate the Doering and Maddey model of water adsorption [102] and all the results were then analyzed according to this surface reconstruction. Only the occurrence of the first STM studies of the water layers on Pt [109, 125] lead to the discovery of more complex reconstructions. Indeed, only in Ref. [109] was the formation of an ordered, continuous two dimensional ice layer observed. Three distinct structural phases were characterized, one of them being an ordered incommensurate ice layer, while the other two are intermediate phases of water molecules with reduced long range order. Following the work of Morgenstern and coworkers, Glebov et al. reported the first LEED characterizations of complex water reconstruction [105]. They showed that water forms two different ordered hexagonal networks with slightly different registry to Pt: as growth proceeds islands with a $\sqrt{37} \times \sqrt{37}R25.3$ (RT37) periodicity form and then restructure into a $\sqrt{39} \times \sqrt{39}R16.1$ (RT39) phase as the surface saturates with water. Although formation of a commensurate hexagonal $\sqrt{3} \times \sqrt{3}R30$ (RT3) structure would allow water to bind in its favoured adsorption site, this would reduce the density of water on the Pt(111) surface and distort the hydrogen bonding structure away from that of an ice Ih(0001) bilayer. Indeed a 7% lateral expansion with respect to an ideal bilayer would be needed to create the $\sqrt{3} \times \sqrt{3}R30$ structure. The strong water-Pt interaction thus lead to a reorganization of the surface layer in order to accommodate as much water molecules as possible, the saturated $\sqrt{39}$ phase being even more compressed than bulk ice (4% lateral compression) [105, 110, 126]. The water desorption rate does not show any noticeable change as the $\sqrt{37}$ to $\sqrt{39}$ compression occurs, indicating this is associated with only a small change in binding energy.

Apart from the kind of network reconstruction, still contradictory results exist

about the vertical distribution of oxygen atoms, the presence of partially dissociated water molecules and the identification of the proton configuration. With respect to this latter point still incoherent results have appeared: some reported a proton ordered network, and seems to identify a promising way to produce proton ordered epitaxial ice [127]. Moreover some IRAS results suggest that very few dangling OH groups point toward the vacuum and from these results an H_{down} configuration was inferred to be the most stable [114]. Nonetheless this conclusions have been challenged subsequently by workfunction measurements on multilayer systems [126]. This experiments showed substantial changes only in the first two layers and proved that thicker systems are indeed proton disordered. The possibility of a partial water dissociation was then proposed to explain the workfunction measurements [111]. Water dissociation was proved to happen in the surface under appropriate conditions: in D or O contaminated surfaces [116, 117], under long LEED exposures [126] or at high temperature for thick systems (for which the first layer is not allowed to desorb) [111]. In all cases it seems that dissociation is an activated process and that the energy barrier is comparable or higher than the one for desorption [111]. No clear indication of the true ground state exists, since at low temperatures metastable structures are virtually stable while at higher temperatures desorption become a competitive process. Nonetheless, partially dissociated structures have been theoretically predicted [93, 122] to be the most stable ones and to be a consequence of the lateral compression of the ice network [123].

7.1.3 Half dissociated water monolayer

The reaction of molecular oxygen with molecular hydrogen on the Pt surface was one of the first evidence of catalysis [128, 129] and a big effort has been devoted in the

last decades in order to elucidate the reaction mechanism. It was proved that two different mechanism exist, depending on the temperature of the system [118]. At high temperatures (above 300 K), higher than the water desorption temperature, oxygen and hydrogen are thought to dissociatively adsorb on the pt surface and directly react in two following steps to from water.

$$O_{(ad)} + H_{(ad)} = OH_{(ad)} \tag{7.1}$$

$$OH_{(ad)} + H_{(ad)} = H_2O_{(ad)} \rightarrow H_2O_{(g)} \tag{7.2}$$

The obtained molecule is then free to leave the substrate, and the reaction is able to proceed. The first step is the reaction limiting step, since it was calculated to have an high activation barrier (0.52 to 0.69 eV [130, 131]). Thus this process is forbidden at temperatures as low as 300 K. Nonetheless water production reaction was proved to occur even at temperatures lower than 170 K with a lower activation energy ($\sim$ 0.13 eV [132]). A different reaction mechanism should be involved at this regime. Indeed the reaction was shown to be characterized by an induction time [132], incompatible with the simplified picture of Eq. 7.1 and 7.2. STM images of the reaction process at low temperature [118, 119] showed that the reaction proceeds through fronts: after a first step in which hydroxyl groups are created on the substrate, an autocatalytic process starts and propagates through the surface.

$$OH_{(ad)} + H_{(ad)} = H_2O_{(ad)} \tag{7.3}$$

$$H_2O_{(ad)} + O_{(ad)} = 2OH_{(ad)} \tag{7.4}$$

The resulting overlayer is a stable and observable reaction intermediate and was characterized to be composed by a regular pattern of hydroxyl groups [119].

The first identification of an hydroxyl overlayer over the Pt surface was done by Fischer and Sexton in 1980 [116]. The system in this case was the results of just Eq. 7.4, namely the dissociation of molecular water on an oxygen covered Pt surface, and therefore it was called the dissociation overlayer. Indeed, a following study demonstrated that the low temperature reaction intermediate is equivalent to the dissociation overlayer [119].

On the basis of TPD experiments involving different isotopes of the oxygen atoms, the stoichiometry of the $H_2O_{(ad)}$+$O_{(ad)}$ reaction was determined to be in agreement with a 2:1 ratio [117]. Still the characterization of the resulting overlayer was done in term of only adsorbed hydroxyl species, since no features of molecular H_2O were observed by HREELS [119]. Thus a reaction mechanism of type

$$2H_2O_{(ad)} + O_{(ad)} = 3OH_{(ad)} + H_{(ad)} \tag{7.5}$$

was proposed [119]. Nonetheless, theoretical calculation [133] showed that the activation energy for this process is too high to be overcome in the low temperature regimes typical of the experiments. A different reaction mechanism was then proposed [133, 134], in which one of the water molecules acts only as a catalyst and does not dissociate

$$2H_2O_{(ad)} + O_{(ad)} = 2OH_{(ad)} + H_2O_{(ad)}. \tag{7.6}$$

The resulting overlayer showed a much higher stability and a lower activation energy with respect to reaction 7.5. Moreover calculated frequency spectra of this overlayer show a good agreement with the experimental HREELS results [134, 135]. The calculated structure presents domains composed by alternating water molecule and hydroxyls adsorbed almost atop. In all the reported structures the oxygen atoms are essentially coplanar and

distributed with a $\sqrt{3}\times\sqrt{3}R30$ periodicity with respect to the substrate. After annealing of the system, molecules eventually reorient to generate a more stable structure characterized by a 3×3 pattern [119]. The excess hydroxyl groups that results from reaction 7.6 form chains at the boundary between the domains, as shown in the STM images of Ref. [119]. This structures decrease the overall stability of the overlayer. Although a $\sqrt{3}\times\sqrt{3}R30$ structure is observed over a range of compositions, the most stable dissociation overlayer [120] was proved to be the one formed by the reaction

$$3H_2O_{(ad)} + O_{(ad)} = 2\left(OH_{(ad)} + H_2O_{(ad)}\right), \tag{7.7}$$

in which the final ratio between OH and H_2O is 1:1.

Finally, from a careful study of the LEED pattern, the 3×3 structure was characterized and was shown to be composed of a an hydrogen bonded pattern in which two thirds of the intermolecular H-bonds are elongated with respect to normal H-bonds while the third is much shorter [121]. Since their contribution to the LEED patterns is too small, it is not possible to identify the distribution of hydrogen atoms inside the cell. Nonetheless intuitively the short H-bonds were attributed to the bonds in which the hydroxyl donates a proton to water. Since the opposite result is obtained from theoretical calculations [136], the attribution of the proton configuration of the layer is still controversial.

7.1.4 Multilayer growth and wetting

Like the water monolayer structure, the characterization of multilayer growth on the Pt surface is also controversial. On the basis of STM studies and TPD, Hodgson and coworkers proposed a model in which the second layer of water nucleates in an ordered array

of crystallites on the $\sqrt{39} \times \sqrt{39}R16$ ice templates [110,126,137,138]. Despite the fact that the intensity of LEED patterns increases with coverage up to >5ML, they ruled out the possibility of an epitaxial layer by layer growth [110]. Indeed the strain in the crystal due to the compressed lattice is too large to allow a stable epitaxial crystal to grow. Instead, single crystallites grow on the substrate, leaving a fraction of the monolayer surface exposed to the vacuum. At higher coverages bulk ice starts to from between crystallites, as shown by the decrease of the $\sqrt{39} \times \sqrt{39}$ LEED pattern [137, 138]. Eventually, at coverages as high as 50 ML, the whole system restructures to from an incommensurate bulk ice $I_h(0001)$ film [138], thus removing the strain associated with the ice/ bulk ice interface at the cost of a less optimum water-Pt interaction.

The inhomogeneous growth of the multilayer structure was further confirmed by other studies [108,139]. A similar picture was drawn in separate studies by Kay and coworkers, on the basis of temperature programmed desorption of rare gases [140–143]. They found that the first water monolayer wets the pt surface [141] and remains partially exposed even at high water coverages [143]. Contrary to Hodgson and coworkers, they found out that the fully coordinated water molecules of the first monolayer result in a hydrophobic surface on which water diffusion is facile [141,143]. The low surface energy of the hydrophobic monolayer relative to the ice surface thermodynamically favors the formation of nonwetting, 3D ice crystallites. This picture was further supported by the observation that kinetically wetted amorphous film dewet upon heating, exposing the water monolayer [142]. Thus, contrary to the model of Hodgson and coworkers, the possibility that the first monolayer acts as a template for the growth of ordered array of crystallites was ruled out. Further-

more, restructuring of the system to form bulk ice does not alter the structure of the first monolayer.

As already pointed out in previous sections, evidences for proton ordered ice films have been reported [127, 144]. In particular Ogasawara et al. showed that a fraction of surface dangling OH bonds greater than 50% is present in multilayer films, in contrast to the statistical value of a proton disordered structure [144]. Moreover, by means of sum frequency vibrational spectroscopy Su et al. provided the evidence for the presence of polar ordering of water molecules [127]. In both cases, proton ordering has been subsequently ruled out. As in the former case, the presence of an high number of dangling OH groups was related to the non uniform structure of the multilayers and the formation of crystallites [138, 143]. As in the case of Ref. [127], it was proved [145] that a small ferroelectric effect of the order of 10^{-4} aligned dipoles could account for the SFG signal and so a completely polarized film is not proved by the reported results. Moreover, the small ferroelectricity was argued to depend only on the inherently asymmetric solid-vacuum interface, and that it is independent of any substrate effect [145].

Finally, dissociation of the first water monolayer buried under thick ice films has been recently reported [111]. The process was shown to occur during high temperature multilayer growth and to be temperature dependent with an activation energy barrier comparable to the single layer desorption energy. The proposed mechanism involves, at the initial stages of the growth process, the formation of H_3O^+/OH^- ions in the first layer, followed by migration and kinetic trapping of H_3O^+ at the ice-vacuum interface. The dissociated structure was shown to be stable up to 200 K even after desorption of the overlaying

water [111].

7.2 Theoretical background

7.2.1 *Ab-initio* calculations: from monomer to intact bilayer

The first studies of water-Pt interaction were done at the Hartree Fock level on minimal clusters composed by five Pt atoms [146]. Despite the complete neglect of the metallic structure of the substrate, these calculations gave substantially correct results for the adsorption energy and geometry: they predict water bonding to occur at atop positions through the oxygen lone-pair orbital and with an equilibrium O-Pt distance of ~ 2.3 Å.

The HF results were confirmed by DFT calculations on periodic systems [92, 94]. Water was shown to absorbs non dissociatively on Pt with an adsorption energy of 0.29 eV to 0.35 eV [92, 94, 114]. DFT results agree with on top adsorption in flat configuration and with an O-Pt distance of ~ 2.4 Å. Water molecules deform little upon adsorption, the OH bond being slightly smaller than the one of a free molecule. Rotation about the O-Pt bond was found to be essentially unhindered: there tends not to be a clear azimuthal preference for H_2O, with different orientations within ~ 0.02 eV of each other [92,94]. Thus it becomes simple for two monomers adsorbed at adjacent atop sites to reorientate and form a dimer. The small decrease in stability due to the unfavorable water-metal interaction is more than compensated by the formation of an hydrogen bond. Rotation in a plane perpendicular to the surface (H_2O tilting) was found to be hindered at low temperatures, the energy barrier for the uprights configuration being as high as $0.14 - 0.19$ eV [93, 94].

Water adsorption in small clusters and chains is more favorable than monomers,

coherently with the experimental findings of STM and TPD at low temperatures [109, 125]. The adsorption energies range from 0.29 eV of the monomers to 0.52 eV of the hexamer [93]. In all the studied cases the O-Pt distance is found to be bimodal with some of the oxygen adsorbed at short distances ($2.4 - 2.7$ Å) and some further from the surface ($2.8 - 3.4$ Å).

Water bilayer on Pt was first studied in the simplified $\sqrt{3} \times \sqrt{3}R30$ periodic cell, with four-six layers of metal atoms and only two water molecules per cell [92, 104, 114]. Thus only proton ordered configurations were considered. The water was supposed to form a puckered hexagonal network as in the bulk ice, with the hydrogen atom not involved in the hydrogen bonds pointing either upward (H_{up}) of to the surface (H_{down}). A partially dissociated structure was also considered, but the adsorption energy was calculated to be much lower than that of the bilayer. All the theoretical calculations agree on the identification of the H_{down} structure as the favoured one. Even if the energy difference between the two configurations is small, this result confirms the observations from vibrational spectroscopies [92]. In the reported vibrational spectra the intensity of the uncoordinated OH group peak is extremely weak compared to that at the ice surface. The H_{down} structure, as well as the H_{up} structure, was found to be almost planar, the average differences between oxygen atoms in the two layers being 0.35 Å and 0.6 Å respectively. Also this result seems to confirm XPS findings [114]. The surface core level shift of Pt 4f surface state and O 1s binding energies suggests that 2/3 of the Pt surface atoms are coordinate to water molecules. This value corresponds to the saturation coverage of the water layer on Pt(111) and thus all the water molecules are coordinated to surface metal atoms [114].

Although almost flat, water molecules in the two layers differ in the number of hy-

drogen atoms participating in the H-bond network [92]. Water in the upper layer donates only one hydrogen atom, as compared to the water molecules in the lower layer that contribute to the network with both hydrogen. This intrinsic asymmetry is reflected in the vibrational amplitude of the different h-bonds, as suggested by calculation of the vibrational spectra for the bilayer reported in Ref. [92]. From calculations it is possible to identify a strong H-bond, characterized by an elongated OH distance (1.0 Å), and two weak h-bonds, characterized by slightly elongated OH distances (0.98 Å) with respect to the free OH (0.97 Å).

All these results were successively questioned by Feibelman [122], as referring to a metastable structure whose adsorption seems to be unfavorable even with respect to bulk ice formation [105]. Indeed, all the calculated adsorption energies were lower that the bulk ice energy formation (0.61 eV) and, as reported previously, experiments showed the RT3 structure not to be the ground state of the system, the RT37 and the RT39 being more stable (the first at low coverages) [105,109,110]. Nonetheless, the calculated energies of the different phases are within the numerical uncertainty of the methods adopted, as proved by the differences in the results obtained with different methods [93,136]. Moreover, DFT does not account for Van der Waals interaction energy, that in the present case can easily overcome the difference. In addition, as pointed out in the work of Michaelides et al. [104], while DFT is able to produce good energy values in different metals that can be compared to each other, this is due in part to a cancellation of errors that works in the same way for each metal. Bulk ice, however, is an insulator, and the exchange-correlation contribution to the energies is very different in the two systems, so that comparison in metals and insulators

is not as reliable. Finally, it is questionable to compare the value of adsorption energy of the thin layer with the bulk energy of ice without considering the energy needed to create interfaces in ice crystallites and within crystallites and the metal surface.

Following the criticism of Feibelman, calculations on the more stable reconstructions were performed [93, 122]. The results agree with the experimental picture, indicating that the RT37 and the RT39 reconstructions are more stable than the RT3 structure for the single monolayer coverage. Nonetheless, analysis of the relative stability of the three phases showed that the RT37 and RT39 structures are less stable as the film thickness increase [93]. At three bilayer coverage, the energies of the three phases are the same within the accuracy of the theoretical treatment. As pointed out in the reply of Meng et al. to Feibelman's comment [122], most of the results obtained for the RT3 structure remain valid for the two other reconstruction: the main differences of these complex systems with respect to the RT3 are the increased densities and the fact that most of the water molecules in the unit cell do not occupy the ideal atop position. As for the latter point, theoretical calculations [94] and XPS results [114] suggest that the water-Pt interaction is not strongly sensitive to the position of the water molecule on the surface. In particular it was shown that, in the optimized adsorption geometry, the water monomer is displaced by ≈ 0.3 Å from the precise atop position and that the cost to move the water molecule from its equilibrium position to the atop position is as low as ~ 0.02 eV [94]. On the other side, core level shifts [114] suggest that all the water molecule in the first layer interact in a similar way with the underlying Pt atoms.

Nonetheless some features peculiar of the RT39 structure emerged from the cal-

culations. In particular it seems that the reduced lattice constant (-7% with respect to that of bulk ice) together with the O-Pt interaction induces spontaneous dissociation of few water molecules (three in Ref. [93, 123]), followed by the formation of separate H_3O^+/OH^- pairs in the unit cell. Even though one of these pairs persisted even in the absence of the substrate, calculation performed by Meng on the RT39 system showed the selfdissociation process between water molecule to be mediated and stabilized by the Pt surface [123].

Ab-initio molecular dynamics simulations performed on these systems and in smaller systems suggest that at finite temperature no significant differences persist between the H_{up} and the H_{down} configuration, the most stable structure being a mixture of both orientations [123, 147]. Moreover, the distribution of oxygen positions along the direction perpendicular to the substrate was shown to be clearly bimodal, with some water molecule attached close to the substrate (distance $<$ 2.5 Å) while the remaining molecules only weakly interact with the pt atoms (distance >3.0 Å) [123]. This theoretical result is clearly at odd with the experimental findings of Ogasawara et al. [114] and call for more in depth investigation.

7.2.2 *Ab-initio* calculations: half dissociated bilayer

As already mentioned in the experimental section, a big contribution to the understanding of the water production reaction came from theoretical calculations of Michaelides and Hu [133,134]. The analysis of the energy barrier of the different processes involved and of the relative stability of the reaction products lead to the assessment of the reaction mechanisms reported in Eq 7.6 in contrast to previous theoretical and experimental interpretations. Calculations were performed using density functional theory on a periodic system with small

(RT3, p2×2, p3×2 and p3×3) unit cells. Despite of the few water molecules and the absence of proton disorder, the authors demonstrated that the stable intermediate of the reaction is an half dissociated bilayer. The reaction pathway was characterized by the autocatalytic role of the water molecule that substantially lower the activation energy for water disproportion [133]. Still using DFT and starting from the half dissociated bilayer, Whanstrom and coworkers were able to reproduce some of the experimental results [135, 148]. Computed vibrational spectra and STM images [135] result in good agreement with experiments. Moreover, Monte Carlo simulations using an ad hoc parametrized interaction potential [148] produced overlayer structure in good agreement with experimental patterns. Some contradicting results still persist as for the characterization of the hydrogen bond network and the localization of protons within the unit cell (see the experimental section) [121, 136].

7.2.3 Classical MD calculations of the water-Pt interface

Most of the processes that happen at the water-metal interface are practically inaccessible to *ab-initio* calculations. The time-scales and length scales involved in phase transitions processes, such as crystallization, formation of crystallite islands, amourphization and restructuring, are too large to be treated with standard *ab-initio* models. In order to model such processes classical molecular dynamics is the reference choice as long as a reliable force field is available for the system under investigation.

To treat metal water interaction many simplified models have been adopted, like the dipolar hard sphere approximation or the Stockmayer model (Lennard-Jones plus point dipole) [149]. However, these models oversimplify the water-water interaction. In order to give a better description of the system and to allow the use of more accurate water

potentials, water-metal interaction was described in the form of pairwise additive potential. Still in most cases the solid is modeled as a molecularly smooth, non polarizable rigid wall (either with Lennard-Jones metal/water potentials, or simply a hard metal-water interaction cutoff) [150–154]. Water in contact with such a wall was shown to posses a peculiar structure at the interface, indicating that the fact that the water network is unavoidably terminated at the interface imposes a significant structural requirement on water molecules and can lead to ice-like boundary conditions.

A first attempt to model with atomistic details water on platinum was done by Spohr and Henzinger using a combination of Lennard-Jones and Coulomb type potentials to describe the Pt atoms at the (0001) surface [155]. Later, a more accurate description of the same surface was formulated in order to include effects such as the surface corrugation of the metal and the orientationally anisotropic water-metal interaction [156]. The potential, written in term of exponential functions, was thus modeled on the basis of barrier for diffusion on the surface and reorientation of the water molecules taken from extended Hückel calculations on a simple cluster [146]. Due to the severe limitation of the Hückel method only the qualitative behavior of the water metal interaction was reproduced. In particular, the Hückel calculation is expected to be reliable only in the region of the potential minimum as for very small distances exchange interactions are not properly taken into account and for larger distances the finite cluster size comes into effect.

The Spohr force field was used to investigate the structure and dynamics of water lamina confined by two Pt surfaces [155, 156], eventually in the presence of an external electric field acting on the molecules [157]. Radial and orientational distributions were

calculated during the MD runs, together with workfunction changes and dielectric properties of water. Simulations showed that the surface induces a structural inhomogeneity in the overlaying water. For molecules at distances up to 10 A from the surface hydrogen bonding and orientation were demonstrated to be strongly affected by the surface.

Starting from the Spohr force-field, Berkowitz and coworkers proposed an analytical form of the water-Pt interaction potential [158]. The rigid force field was also adapted to treat the Pt(111) surface [159]. The simplified water-surface interaction potential together with the inexpensive SPC/E force field for water allowed for simulation of bigger systems and longer timescales. Using this method, Berkowitz and coworkers were able to identify a solid like behavior of water molecules in contact with the substrate even at relatively high temperatures (300 K) [159–162]. Moreover, a structural phase transition from liquid water to cubic ice was demonstrated to occur under the presence of an external electric field induced by an uniform charge density spread over the pt surfaces [163].

Despite the number of results obtained, both the Spohr and Berkowitz interaction potentials have not been successfully used to model the structure of the first layers of water on Pt at low temperatures. The structure of the water overlayer was always found to resemble those of the underlying substrate [157, 161]. Thus on the Pt(111) surface only the simplest RT3 bilayer reconstruction was observed. This result is coherent with the inclusion in the force fields of only the main features of the water-Pt interaction. Indeed most of the peculiar features of those systems were demonstrated by *ab-initio* calculations to be the results of a complex balance between hydrogen bonding and water-Pt interaction [104, 123]. In particular, the occurrences of water selfdissociation and of strong Pt-O bond

are incompatible with standard force fields.

Finally it is worth mentioning some classical MD simulations of water clusters, adlayers and crystals on virtual metal surfaces [164–167]. In these studies the effects of the metal surface is completely neglected apart from the geometrical constraint on the adsorbed water molecules. In this way, by fixing one of the two effects that drive interfacial phenomena (water-metal interaction), different results on the remaining one (water-water interaction) were obtained. In particular the consequences of metal surface constraints on the hydrogen bond strength and cooperativity were analyzed by Lankau et al in several works [164, 168–171]. In addition Witek and Buch studied the effects of the metal induced order in the first bilayer of water [165]. The decay mechanism of ferroelectricity (proton order) and the influence of the first bilayer flattening on the adsorbate structure were characterized in depth. A new kind of defect in the ice structure was reported and shown to provide a mechanism for decay of ferroelectricity over the range of 2-3 bilayers only. Flattening of the bottom layer results in sandwich like adsorbate structures and in the disappearing of most of the dangling OH bond from the upper surface.

Chapter 8

The effect of proton disorder

8.1 Introduction

As we have seen in the preceding chapters, the characterization of water overlayer on the Pt (111) surface is still controversial.

In particular the effect of proton disorder, both in plane and out of plane, steel need deeper investigations. Indeed proton disorder is known to be essential to stabilize not only bulk crystals, but also crystalline films [172]; moreover it has been already supposed to play an important role in determining the wetting structures on transition metals surfaces [98, 101, 120]. On the Pt(111) surface a systematic study of such effect is still missing: experimental results suggest a proton ordered phase to be the most stable phase in the half dissociated overlayer, while no clear evidence for proton order/disorder has been put forward on the intact bilayer.

In addition, the theoretical characterization of the water overalyer structure does not completely agree with some experimental results: in particular the evidence for the

presence of short and strong water-metal bonds still needs to be theoretically confirmed.

To address these problems, we choose to use a large unit cell, since it allows for proton disordered configurations and for a less biased search of the lowest energy structure (as underlined in Ref. [147]). We show that for this kind of system the proton disorder is essential to understand the ground state structure. In addition, we show that the simple inclusion of full proton disorder allows structures in which some of the water molecules form a strong bond with the substrate to be obtained, leading to a short bonding distance (2.3 Å) in agreement with experimental results. The formation of these strong bonds leads to a weakening of the hydrogen-bond network and the remaining molecules move to a larger distance (3.1-3.5 Å). From such results a deeper insight into the water bilayer adsorption mechanism is gained. The interplay between the hydrogen-bond network weakening and the formation of bonds with the surface is further elucidated by adsorbing the ground state structure onto Ag(111), which is almost inert to water adsorption.

8.2 Computational details

We use the DFT based finite-electronic temperature method (FEMD) [173] implemented in the plane-wave based CPMD code [59]. In this method the electron density and the Hellman-Feynman forces are determined via a subspace diagonalization of the high temperature electron density matrix. The subspace is expanded in a plane-wave basis set that in our set-up is cutoff at 60 Ry, a value which, according to our previous work [96], is sufficient to describe satisfactorily the molecule/metal interaction. We use pseudo-potentials generated according to Troullier-Martins [60] scheme; all the pseudo-potentials were accur-

ately tested to reproduce bulk and surface properties of the metal, and correct structural properties for the molecule. We use the PBE [174] generalized gradient corrected functional. The prototype system consists of a (111) surface of platinum represented by 3 and 4 layers (as explained later on regarding the geometry optimization procedure) and a layer of water composed of 24 molecules. We employ a 6×6 supercell of hexagonal symmetry with the cell dimension in the direction perpendicular to the surface equal to 25.5 Å so that the thickness of the vacuum between the water molecules and the bottom layer of the image slab of Pt(111) is equal to about 15 Å; due to the extended size of the box, we performed the calculations at the Γ-point approximation. Geometry optimizations, using the BFGS algorithm, were done first with only 3 layers until the maximum component of the ionic forces was below 2×10^{-3} atomic units, then we add a fourth layer and further optimize the structure until the convergence of the root-mean square force was below 10^{-3} atomic units, the maximum component of the ionic force was at least below 3×10^{-3} and the energy changes were below 0.01 eV, i.e. about 10^{-4} eV per molecule into the adsorption energy of water.

8.3 Structures

The initial configuration of the water film is the one of an ideal (0001) bilayer of hexagonal ice stretched in the xy plane so as to match the surface lattice parameter of the metal. In the case of Pt the mismatch between the two ideal lattices is $\sim 8\%$. All the oxygen atoms are located at atop sites, with coverage 2/3 ML. In this respect our 6x6 supercell is a 12-fold replica of the RT3 structure. Even though it is not the most thermodynamically

stable, the RT3 configuration has been observed experimentally [109, 175]. In addition this choice gives us the advantage that a direct comparison with other metal surfaces can be made for which the RT3 is the standard adsorption structure, e.g. Ag(111), Pd(111) and Rh(111).

The use of an extended cell allows in-plane and out-of-plane proton disorder to be included in the system. Five different proton arrangements are considered: a fully proton-ordered configuration (H^{ord}_{down}), similar to the ones already studied in literature, two in-plane proton-disordered structures (H_{up} and H_{down}) and two fully proton disordered structures, one dissociated (H_{diss}) and one undissociated (H_{mix}). Following the convention of previous works [104] we define H_{up} and H_{down} as the configuration where the hydrogen atoms not participating in a hydrogen-bond point toward the vacuum or metal surface, respectively. The proton disordered configurations have been generated by a Montecarlo method [81], so to minimize either the global or the in-plane dipole moment. Obviously the z component of the dipole moment can be set to zero only if there is no constraint on the number of protons pointing toward the metal surface: in this case we have the so called H_{mix} film. We stress that the proposed H_{mix} structure is just one configuration in a virtually infinite ensemble of proton disordered configurations, which cannot be explored by present day computational resources. The most stable proton disordered water adlayer should be obtained by a procedure that optimizes the rate between hydrogen up and down and as a consequence the amount of strong water-metal bonds and hydrogen bonds. In the initial configurations the water molecules are on the top sites of the platinum surface, the vertical separation between the oxygen atoms in the water bilayer is 0.6 Å, and the lower

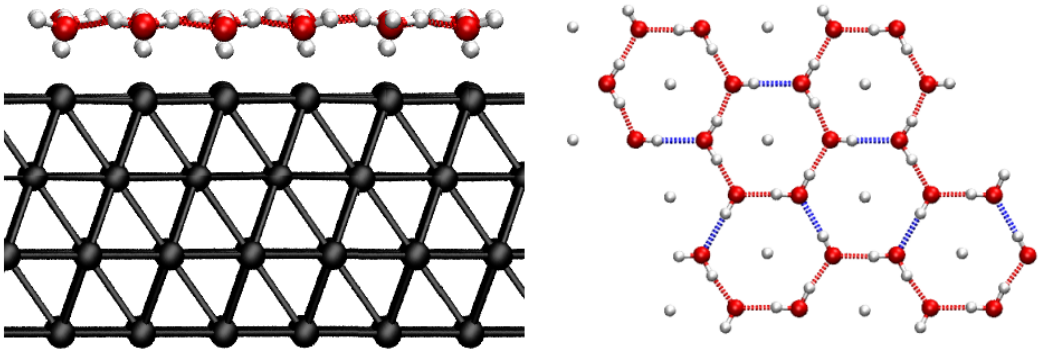

Figure 8.1: Side and top views of the proton disordered H_{diss} configuration. Hydrogen bonds are drawn in red (blue) when the O-O distance is smaller (greater) than 3.0 Å (see the text).

layer is 2.6 Å apart from the metal slab. In the partially dissociated configuration (H_{diss}), the dissociated protons sit at the free top sites. In Fig. 8.1-8.5 the final geometries of the different systems are reported.

8.4 Results

The total adsorption energies per molecule are computed as $E_{ads} = (E_{tot} - E_{Pt} - 24E_{H_2O})/24$, where E_{tot} is the energy of the optimized Pt+water film system, E_{Pt} the energy of the bare Pt surface and E_{H_2O} the energy of a water molecule. The values are reported in Tab. 8.1 and show very good agreement with those of Ref. [104] as for the H^{ord}_{down}. In order to characterize the tendency of the hydrogen bonding network to become less tight as a result of the chemical interaction with the surface, we monitor the number of "strong" hydrogen bonds. An H-bond is defined as "strong" when the O-O distance is smaller than 3.0 Å. In the initial configurations this distance is 2.98 Å.

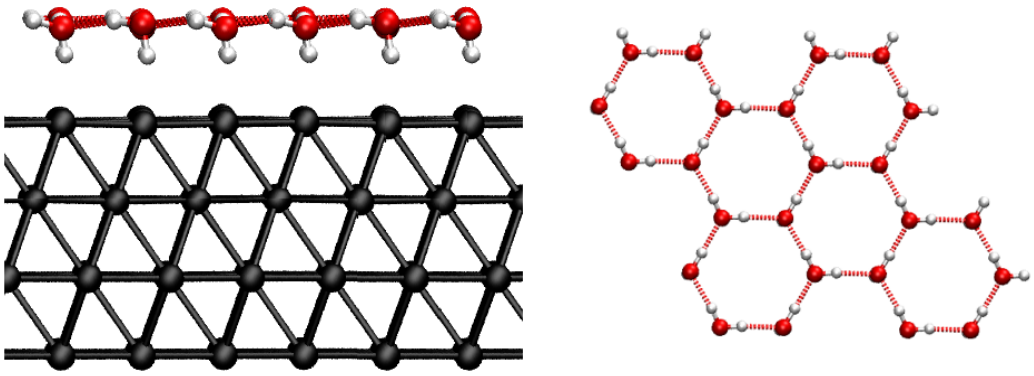

Figure 8.2: Side and top views of the proton ordered H_{down} configuration.

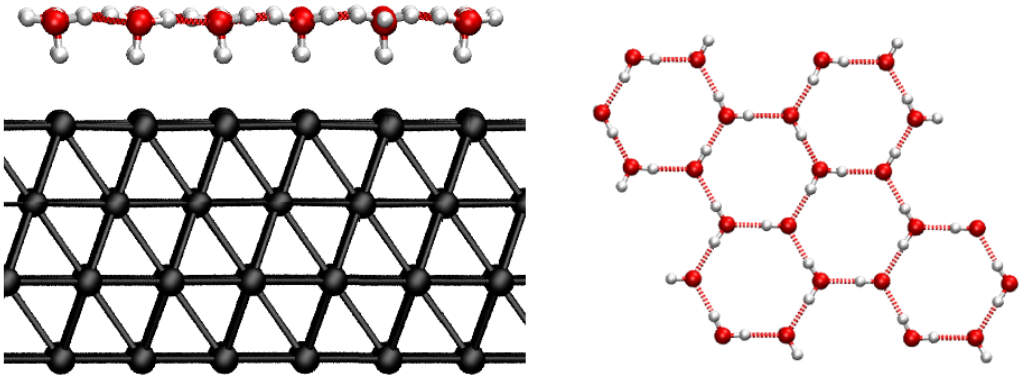

Figure 8.3: Side and top views of the in-plane proton disordered H_{down} configuration.

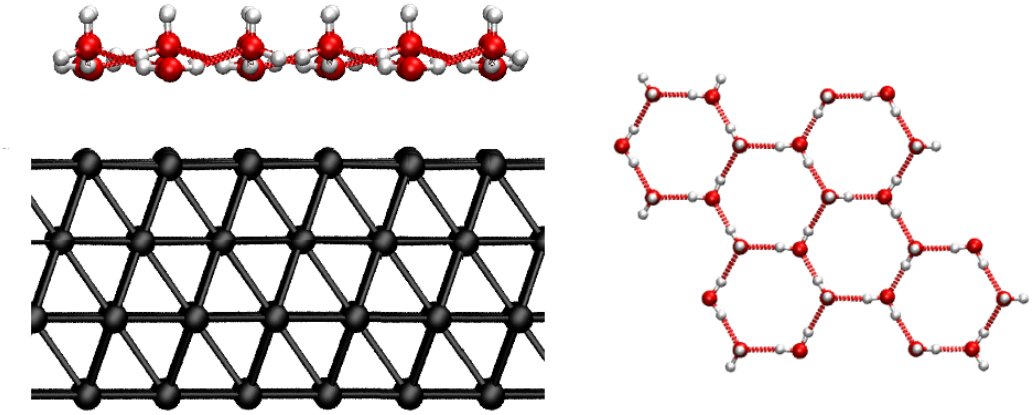

Figure 8.4: Side and top views of the in-plane proton disordered H_{up} configuration.

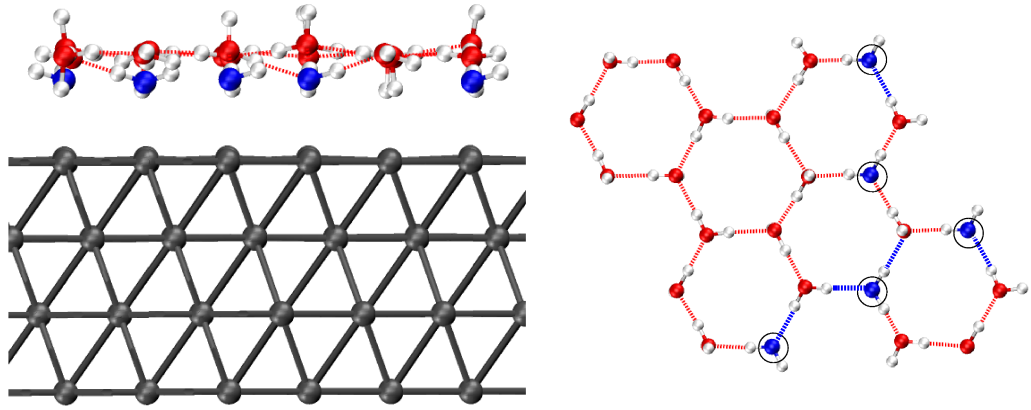

Figure 8.5: Side and top views of the proton disordered H_{mix} configuration. The five Pt atoms bonded to the oxygen atoms are raised by 0.1 Å with respect to the average z position of the remaining 31 first-layer Pt atoms. The five bonded oxygen atoms (circled in top view) stay at 2.33 Å from the closest Pt atoms, while the rest of the water network lies 3.1-3.4 Å away from the surface. Hydrogen bonds are drawn in red (blue) when the O-O distance is smaller (greater) than 3.0 Å (see the text).

In the all the undissociated structures, but H_{mix}, the H-bond network stiffens during the optimization. All the H-bonds shorten, so to recover the ideal O-O distance ($\sim$ 2.78 Å). Since the underlying metal surface acts as a topological confinement, this process (i.e. O-O shortening) is achieved via a reduction of the vertical spacing of the bilayer (initially as long as 0.9 Å). The water bilayers relax at a rather large distance from the Pt surface. In these configurations they do not interact chemically with the surface, as confirmed by the charge density plot in Fig.8.6.

In H_{diss} both the OH groups and the undissociated H_2O bind chemically to the metal surface and form a H-bond pattern where strong (O-O distance: 2.6 Å) and very elongated (3.1 Å) H-bonds alternate. This picture, confirmed by experiments [121] and previous calculations [136], suggests a competition between the chemical O-Pt bonding and the strength of the H-bond network.

This balance determines the adsorption mechanism of the H_{mix} adlayer, which is by far the most stable of the configurations investigated. Due to the full proton disorder, the system is less constrained. This enhanced flexibility allows the optimal balance to be achieved by sacrificing some of the hydrogen-bond energy of the two dimensional water adlayer network (top panel of Fig. 8.7) and gaining chemical energy with the formation of stronger water-metal bonds. Although the periodicity constraints are relaxed, the water molecules maintain the initial ordered arrangement in the xy plane, while the distribution of vertical heights is clearly bimodal (bottom panel of Fig. 8.7). The majority of water molecules (80%) form a flat overlayer where the Pt-O distance is distributed between 3.2 and 3.5 Å, while the flat water molecules of the bottom layer bind tightly to Pt atoms at

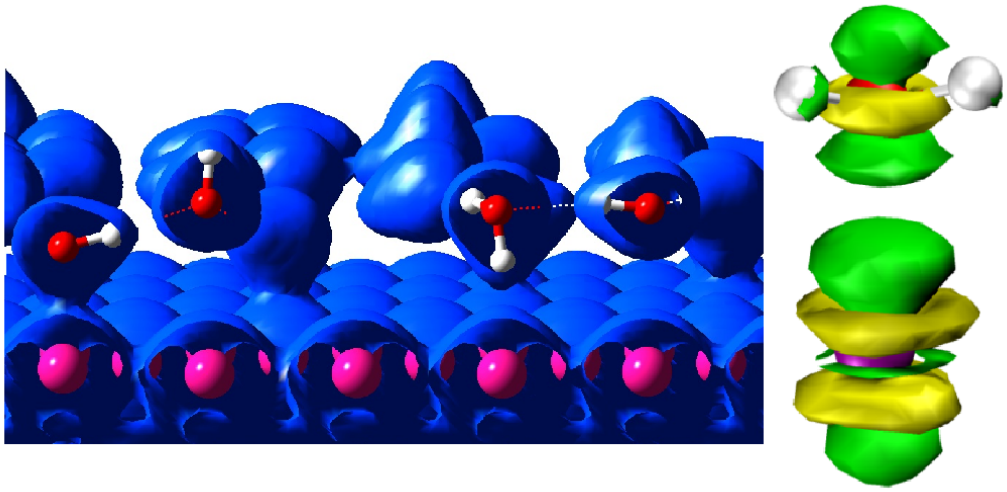

Figure 8.6: Electron density profiles for the H_{mix} case. The four possible configurations of water molecules are shown in the left panel (the iso-surface level is 0.270 $e/\text{Å}^3$). From left to right: a flat water molecule in the bottom layer forming a O-Pt bond, a water molecule with a hydrogen atom pointing to the vacuum, a water molecule forming a hydrogen bond with the surface and a flat water molecule in the top layer displaying no interaction with the surface. Right panel: electron density difference maps for one of the flat water molecules in the bottom layer, adsorbed via O-Pt bond. The green (yellow) surface indicates depletion (accumulation) of electronic density of 0.036 $e/\text{Å}^3$. Note that this snapshot compares very well to the monomer adsorption electron density difference maps shown in Ref. [94].

a distance of ∼2.3 Å. The electronic density profiles for the latter molecules (see the right panel in Fig. 8.6) shows the formation of chemical bonds with the surface which are much stronger than in the other structures. Moreover the electron density difference of the Pt-Me bonding for the H_{mix} case (left panel in Fig. 8.6) shows a strong chemical bond resembling that of an isolated monomer [94], i.e. the ideal conformation for the molecular adsorption. This comparison proves that the molecule-surface interaction of those water molecules that are adsorbed via O-Me bond, is almost exactly the same as for an isolated monomer in the same position. As a chemical bond is established between metal and oxygen atoms, the hydrogen bonding of the water adlayer is weakened, as proven by the elongation of a number of hydrogen bonds occurring during the optimization of the H_{mix} system (Fig. 8.7).

In order to provide further evidence of the interplay between Pt-O chemical bond and the stiffness of the hydrogen bonding network in the H_{mix} system, we substituted Pt with Ag, which has a substantially smaller affinity to the adsorption of water [94]. In this manner the metal-oxygen chemical bond is weakened, and performing the geometry optimization we observe the up-shifting of the previously chemisorbed flat H_2O molecules and the restoration of a tight H-bond network (Fig. 8.7). Computational details are the same as for the other systems treated here. For Ag we use an LDA pseudo-potential previously tested according to the criteria employed in this work. The final O-O distances for H_{mix} configuration on Pt, was scaled according to the lattice constant of Ag, and, as a consequence, the same is done when counting hydrogen bonds. The calculated adsorption energy of -0.46 eV is in good agreement with the ones reported for proton ordered systems in Ref. [104]. This means that for metal surfaces with low water affinity the issue of proton

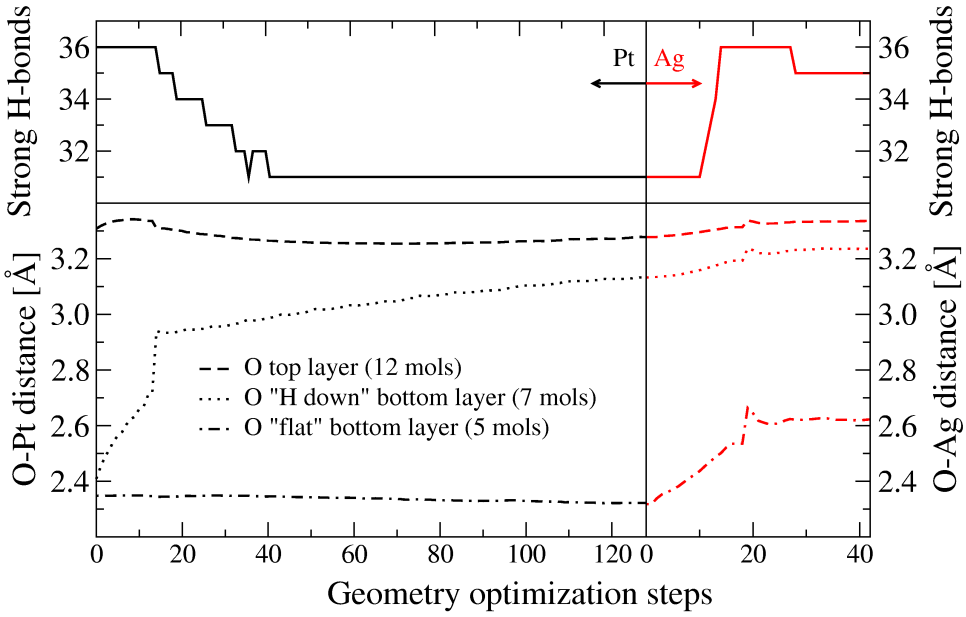

Figure 8.7: Top panels: the number of "strong" hydrogen bonds during the geometry optimization process for the H_{mix} case on Pt (Ag) surface is reported on the left (right) side. Bottom panels: Evolution of the distances from the metal surface of the water molecules for the H_{mix} configuration. In the left (right) panel we show the distance from the Pt (Ag) surface of the oxygen of the top water layer (dashed line), of the oxygen of the H_{down} water molecules in the bottom layer (dotted line), and (dashed-dotted line) of the "flat" water molecules, i.e. those circled in Fig. 8.5.

disorder is not relevant.

While providing novel insights about the adsorption mechanism, it is also remarkable that the H_{mix} on Pt is the only configuration that accounts for the x-ray absorption/photoemission spectroscopy measurements in [114], indicating a relatively strong Pt-O bonding, with a layer of oxygen atoms 2.3–2.4 Å far from the surface. It must be noticed that, such a short Pt-O bond has not been observed in any of the other undissociated structures considered in this work or in the many previously reported calculations [92,93,104,114].

	E_{ads}	O-H-Pt	O-Pt	H-O-Pt	OH-Pt
H^{ord}_{down}	-0.49	3.1	2.8	-	-
H_{down}	-0.50	3.2	3.1	-	-
H_{up}	-0.48	-	2.9	3.5	-
H_{mix}	-0.53	3.2	2.3/3.2	3.3/3.5	-
H_{diss}	-0.29	-	2.2	-	2.1

Table 8.1: The adsorption energies (in eV) and the distances between oxygen and platinum (in Å) are here reported for the 5 systems we studied. The labels of the columns have to be interpreted as follows: O-H-Pt the water molecule has a proton that points toward the Pt surface, O-Pt the water molecule is flat with respect to the metal surface, H-O-Pt the water molecule has a proton that points toward the vacuum, OH-Pt refers to a dissociated OH group.

Conclusions

In the present work we analyzed the structure of water overlayers in two different systems. In the first part of the work a thick ice overalyer on a chlorine terminated silicon substrate was studied. As a first step a simplified system was investigated by *ab-initio* simulations. These were subsequently used to model a classical water-substrate interaction potential that allowed to treat realistic systems and to reproduce experimental results with an overall good agreement. The analysis of the atomistics features underlying the experimental evidences lead a significant understanding of the reorganization processes that happen in interfacial ice under ultrafast heating. Two processes were seen to contribute to the experimental behavior of the structure factor, namely the formation of topological defects and the elongation of hydrogen bonds in the direction orthogonal to the substrate. Of these processes, the former is particularly interesting since it was shown to be almost irreversible over a time scale of nanoseconds and because it is known to mediate melting processes. Thus it has fundamental implications on the thermodynamic stability of crystal phases.

The second part of the thesis is an attempt to contribute to the understanding of the structure of a single layer of water molecules on top of a platinum substrate. The

problem is very complex and was the subject of many studies: different controversial results appeared in the literature, both experimental and theoretical. In order to elucidate the final structure and to explain experimental results, detailed calculations are needed. Indeed, for this kind of systems only *ab-initio* calculations are able to model the different physical effects that come into play, in particular the subtle interplay between the formation of a metal-oxygen bond and the water-water hydrogen bonding. In addition, in order to get a picture close to the experimental evidences, relaxed periodic boundary conditions and large system sizes were soon pointed out to be necessary. In our work we were able to further elucidate the influence of the different physical aspects in the determination of the optimal structure. We chose to focus on the effect of proton order and we showed that, although it is often considered a minor issue, it has a significant influence on the final structure of the adsorbed water monolayer. Indeed, the formation of strong water-Pt bonds was shown to be possible only when completely proton disordered configurations are considered. The formation of these bonds is in agreement with some experimental results on the system and lead to a global stabilization of the overalyer at the expense of the water-water interaction, the resulting water overalyer showing a bimodal height distribution. Finally, the importance of proton order was related to the affinity of the water molecules to the metal surface. By substituting platinum with silver, that shows a substantially low water affinity, proton disorder was shown to have a negligible influence.

In summary, by means of *ab-initio* and classical simulations we were able to add and explain some important details on the complex array of phenomena that characterizes the structure of water at interfaces.

Acknowledgement

For all the 'science' present in this thesis there are few important people that I want to acknowledge. I would like to acknowledge Michele for supervising me on this work and on all the other works that have not appeared in this thesis. I want to acknowledge Davide Donadio for his help and supervision on the first part of my Ph.D. and for his suggestions and his assistance on the last part. I am very pleased to acknowledge Professor Zewail for his contributions to the first part of this thesis and I am also grateful to Luigi Delle Site and Luca Ghiringhelli for letting me participate in their study.

For everything in this thesis but science I want to acknowledge the important people of my life. There is not enough space to acknowledge Katia as she deserves, but I want to acknowledge her for being the only one able to change and mitigate the bad sides of my character in almost every occasion and to support me in all the other occasions. I want to acknowledge my parents and my brother Tommaso, for being there, always. I want to acknowledge my grandparents, for being always proud of their grandson.

Bibliography

[1] Thiel, P. A.; Madey, T. E. *Surf. Sci. Rep.* **1987**, *7*, 211–385.

[2] Henderson, M. A. *Surf. Sci. Rep.* **2002**, *46*, 1–308.

[3] Verdaguer, A.; Sacha, G. M.; Bluhm, H.; Salmeron, M. *Chem. Rev.* **2006**, *106*, 1478–1510.

[4] Ewing, G. E. *Chem. Rev.* **2006**, *106*, 1511–1526.

[5] Srinivasan, R.; Lobastov, V. A.; Ruan, C.-Y.; Zewail, A. H. *Helv. Chim. Acta* **2003**, *86*, 1763–1838.

[6] Srinivasan, R.; Feenstra, J. S.; Park, S. T.; Xu, S.; Zewail, A. H. *J. Am. Chem. Soc.* **2003**, *126*, 2266–2267.

[7] Ruan, C.-Y.; Yang, D.-S.; Zewail, A. H. *J. Am. Chem. Soc.* **2004**, *126*, 12797–12799.

[8] Vigliotti, F.; Chen, S.; Ruan, C.-Y.; Lobastov, V. A.; Zewail, A. H. *Angew. Chem. Int. Ed.* **2004**, *43*, 2705–2709.

[9] Ruan, C.-Y.; Lobastov, V. A.; Vigliotti, F.; Chen, S.; Zewail, A. H. *Science* **2004**, *304*, 80–84.

[10] Keating, P. N. *Phys. Rev.* **1966**, *145(2)*, 637–645.

[11] Stillinger, F. H.; Weber, T. A. *Phys. Rev. B* **1985**, *31*, 5262.

[12] Biswas, R.; Hamann, D. R. *Phys. Rev. Lett.* **1985**, *55*, 2001.

[13] Tersoff, J. *Phys. Rev. Lett.* **1986**, *56*, 632.

[14] Tersoff, J. *Phys. Rev. B* **1988**, *37*, 6991.

[15] Tersoff, J. *Phys. Rev. B* **1988**, *38*, 9902.

[16] Bazant, M. Z.; Kaxiras, E. *Phys. Rev. Lett.* **1996**, *77*, 4307.

[17] Bazant, M. Z.; Kaxiras, E.; Justo, J. F. *Phys. Rev. B* **1997**, *56(14)*, 8542–8552.

[18] Wallqvist, A.; Mountain, R. D. *Rev. Comput. Chem.* **1999**, *13*, 183–247.

[19] Guillot, B. *J. Mol. Liquids* **2002**, *101*, 219–260.

[20] Jorgensen, W. L.; Tirado-Rives, J. *Proc. Natl. Acad. Sci. USA* **2005**, *102*, 6665–6670.

[21] Bansal, A.; Li, X.; Yi, S. I.; Weinberg, W. H.; Lewis, N. S. *J. Phys. Chem. B* **2001**, *105*, 10226–10277.

[22] Eves, B. J.; Lopinski, G. P. *Surf. Sci.* **2005**, *579*, L89–L96.

[23] Biering, S.; Hermann, A.; Schmidt, W. G. *Phys. Rev. B* **2006**, *73*, 235429(6).

[24] Silvestrelli, P. L.; Toigo, F.; Ancillotto, F. *J. Phys. Chem. B* **2006**, *110*, 12022–12028.

[25] Schluter, M.; Rowe, J. E.; Margaritondo, G.; Ho, K. M.; Cohen, M. L. *Phys. Rev. Lett.* **1976**, *37(24)*, 1632–1635.

[26] Rowe, J. E.; Margaritondo, G.; Christman, S. B. *Phys. Rev. B* **1977**, *16(4)*, 1581–1589.

[27] Pandey, K. C.; Sakurai, T.; Hangstrum, H. D. *Phys. Rev. B* **1977**, *16(8)*, 3648–3651.

[28] Larsen, P. K.; Smith, N. V.; Schlüter, M.; Farrell, H. H.; Ho, K. M.; Cohen, M. L. *Phys. Rev. B* **1978**, *17(6)*, 2612–2619.

[29] Schlüter, M.; Rowe, J. E.; Weeks, S. P.; Christman, S. B. *J. Vac. Sci. Technol.* **1978**, *16(2)*, 615–617.

[30] Citrin, P. H.; Rowe, J. E.; Eisenberger, P. *Phys. Rev. B* **1983**, *28(4)*, 2299–2301.

[31] Schnell, R. D.; Rieger, D.; Bogen, A.; Himpsel, F. J.; Wandelt, K.; Steinmann, W. *Phys. Rev. B* **1985**, *32(12)*, 8057–8065.

[32] Schlüter, M.; Cohen, M. L. *Phys. Rev. B* **1978**, *17(2)*, 716–725.

[33] Mednick, K.; Lin, C. C. *Phys. Rev. B* **1978**, *17(12)*, 4807–4820.

[34] Bachelet, G. B.; Schluter, M. *J. Vac. Sci. Technol. B* **1983**, *1(3)*, 726–728.

[35] Seel, M.; Bagus, P. S. *Phys. Rev. B* **1983**, *28(4)*, 2023–2038.

[36] Bachelet, G. B.; SChlüter, M. *Phys. Rev. B* **1983**, *28(4)*, 2302–2304.

[37] Dev, B. N.; Mishra, K. C.; Gibson, W. M.; Das, T. P. *Phys. Rev. B* **1984**, *29(2)*, 1101–1103.

[38] Illas, F.; Rubio, J.; Ricart, J. M. *Phys. Rev. B* **1985**, *31(12)*, 8068–8075.

[39] van den Hoek, P. J.; Ravenek, W.; Baerends, E. J. *Phys. Rev. B* **1988**, *38(17)*, 12508–12513.

[40] Mohapatra, S. M.; Dev, B. N.; Mishra, K. C.; Sahoo, N.; Gibson, W. M.; Das, T. P. *Phys. Rev. B* **1988**, *38(17)*, 12556–12566.

[41] Ricca, A.; Musgrave, C. B. *Surf. Sci.* **1999**, *430*, 116–125.

[42] Blomquist, T.; Kirczenow, G. *Phys. Rev. B* **2006**, *73(19)*, 195303(10).

[43] Rowe, J. E. *Phys. Rev. Lett.* **1975**, *34*, 398.

[44] Rowe, J. E. *Surf. Sci.* **1975**, *53*, 461.

[45] Bansal, A.; Li, X.; Lauermann, I.; Lewis, N. S. *J. Am. Chem. Soc.* **1996**, *118*, 7225–7226.

[46] Gao, Q.; Cheng, C. C.; Chen, P. J.; Choyke, W. J.; Yates, J. T. *J. Chem. Phys.* **1993**, *98*, 8380.

[47] Terry, J.; Mo, R.; Wigren, C.; Cao, R.; Mount, G.; Pianetta, P.; Linford, M. R.; Chidsey, C. E. D. *Nucl. Instrum. Methods Phys. Res. B* **1997**, *133*, 94.

[48] Zhu, X. Y.; Boiadjiev, V.; Mulder, J. A.; Hsung, R. P.; Major, R. C. *Langmuir* **2000**, *16*, 6766.

[49] Li, Z.; Kamins, T. I.; Li, X.; Williams, R. S. *Surf. Sci.* **2004**, *554*, L81.

[50] Lopinski, G. P.; Eves, B.; Hul'ko, O.; Mark, C.; Patitsas, S. N.; Boukherroub, R.; Ward, T. R. *Phys. Rev. B* **2005**, *71*, 125308(4).

[51] Gaussian 03, Revision C.02. Frisch, M. J.; Trucks, G. W.; Schlegel, H. B.; Scuseria, G. E.; Robb, M. A.; Cheeseman, J. R.; Montgomery, Jr., J. A.; Vreven, T.; Kudin, K. N.; Burant, J. C.; Millam, J. M.; Iyengar, S. S.; Tomasi, J.; Barone, V.; Mennucci, B.; Cossi, M.; Scalmani, G.; Rega, N.; Petersson, G. A.; Nakatsuji, H.; Hada, M.; Ehara, M.; Toyota, K.; Fukuda, R.; Hasegawa, J.; Ishida, M.; Nakajima, T.; Honda, Y.; Kitao, O.; Nakai, H.; Klene, M.; Li, X.; Knox, J. E.; Hratchian, H. P.; Cross, J. B.; Bakken, V.; Adamo, C.; Jaramillo, J.; Gomperts, R.; Stratmann, R. E.; Yazyev, O.; Austin, A. J.; Cammi, R.; Pomelli, C.; Ochterski, J. W.; Ayala, P. Y.; Morokuma, K.; Voth, G. A.; Salvador, P.; Dannenberg, J. J.; Zakrzewski, V. G.; Dapprich, S.; Daniels, A. D.; Strain, M. C.; Farkas, O.; Malick, D. K.; Rabuck, A. D.; Raghavachari, K.; Foresman, J. B.; Ortiz, J. V.; Cui, Q.; Baboul, A. G.; Clifford, S.; Cioslowski, J.; Stefanov, B. B.; Liu, G.; Liashenko, A.; Piskorz, P.; Komaromi, I.; Martin, R. L.; Fox, D. J.; Keith, T.; Al-Laham, M. A.; Peng, C. Y.; Nanayakkara, A.; Challacombe, M.; Gill, P. M. W.; Johnson, B.; Chen, W.; Wong, M. W.; Gonzalez, C.; Pople, J. A.

[52] VandeVondele, J.; Krack, M.; Mohamed, F.; Parrinello, M.; Chassaing, T.; Hutter, J. *Comp. Phys. Comm.* **2005**, *167*.

[53] Hohenberg, P.; Kohn, W. *Phys. Rev. B* **1964**, *136*, 864.

[54] Kohn, W.; Sham, L. J. *Phys. Rev. A* **1965**, *140*, 1133.

[55] Becke, A. D. *Phys. Rev. A* **1988**, *38*, 3098.

[56] Lee, C.; Yang, W.; Parr, R. G. *Phys. Rev. B* **1988**, *37*, 785.

[57] Gödecker, S.; Teter, M.; Hutter, J. *Phys. Rev. B* **1998**, *54*, 1703.

[58] Hartwigsen, C.; Gödecker, S.; Hutter, J. *Phys. Rev. B* **1998**, *78*, 3641.

[59] CPMD, version 3.10.5. Hutter, J.; *et al.*.

[60] Troullier, N.; Martins, J. L. *Phys. Rev. B* **1991**, *43*, 1993.

[61] Bayly, C.; Cieplak, P.; Cornell, W.; Kollman, P. A. *J. Phys. Chem.* **1993**, *97*, 10269.

[62] Odde, S.; Mhin, B. J.; Lee, S.; Lee, H. M.; Kim, K. S. *J. Chem. Phys.* **2004**, *120(20)*, 9524–9535.

[63] Jorgensen, W. L.; Chandrasekhar, J.; Madura, J. D.; Impey, R. W.; Klein, M. L. *J. Chem. Phys.* **1983**, *79*, 926–935.

[64] Sanz, E.; Vega, C.; Abascal, J. L. F.; MacDowell, L. G. *Phys. Rev. Lett.* **2004**, *92*, 255701(4).

[65] Vega, C.; Sanz, E.; Abascal, J. L. F. *J. Chem. Phys.* **2005**, *122*, 114507(9).

[66] van der Spoel, D.; Buuren, A. R.; Tieleman, D. P.; Berendsen, H. J. C. *J. Biomol. NMR* **1996**, *8*, 229.

[67] Smith, W.; Forester, T. *J. Mol. Graphics* **1996**, *14*, 136.

[68] Berendsen, H. J. C.; Postma, J. P. M.; van Gusteren, W. F.; Nola, A. D.; Haak, J. R. *J. Chem. Phys.* **1984**, *81*, 3684.

[69] Hautman, J.; Klein, M. L. *Mol. Phys.* **1992**, *75*, 379.

[70] Essmann, U.; Perera, L.; Berkowitz, M. L.; Darden, T.; Lee, H.; Pedersen, L. G. *J. Chem. Phys.* **1995**, *103*, 8577.

[71] Steinhardt, P. J.; Nelson, D. R.; Ronchetti, M. *Phys. Rev. B* **1983**, *28(2)*, 784–805.

[72] Radhakrishnan, R.; Trout, B. *J. Am. Chem. Soc.* **2003**, *125*, 7743–7747.

[73] Radhakrishnan, R.; Trout, B. *Phys. Rev. Lett.* **2003**, *90*, 158301(4).

[74] Jedlovzky, P.; Vincze, A.; Horvai, G. *Phys. Chem. Chem. Phys.* **2004**, *6*, 1874.

[75] Liu, P.; Harder, E.; Berne, B. J. *J. Phys. Chem. B* **2004**, *108*, 6595–6602.

[76] Donadio, D.; Raiteri, P.; Parrinello, M. *J. Phys. Chem. B* **2005**, *109*, 5421.

[77] R.Martonak.; Donadio, D.; Parrinello, M. *Phys. Rev. Lett.* **2004**, *92*, 225702(4).

[78] Martonak, R.; Donadio, D.; Parrinello, M. *J. Chem. Phys.* **2005**, *122*, 13501(10).

[79] Yuan, X.; Cormack, A. N. *Comp. Mat. Sci.* **2002**, *24*, 343–360.

[80] Raiteri, P.; Laio, A.; Parrinello, M. *Phys. Rev. Lett.* **2004**, *93*, 087801(4).

[81] Buch, V.; Sandler, P.; Sadlej, J. *J. Phys. Chem. B* **1998**, *102*, 8641.

[82] LAio, A.; Parrinello, M. *Proc. Natl. Acad. Sci. USA* **2002**, *99*, 12562–12566.

[83] Iannuzzi, M.; Laio, A.; Parrinello, M. *Phys. Rev. Lett.* **2003**, *90*, 238302(4).

[84] Laio, A.; Rodigruez-Fortea, A.; Gervasio, F. L.; Ceccarelli, M.; Parrinello, M. *J. Phyc. Chem. B* **2005**, *109*, 6714–6721.

[85] Huber, T.; Torda, A. E.; van Gusteren, W. F. *J. Comput.* **1994**, *8*, 695–708.

[86] Gear, C. W.; Kevrekidis, I. G.; C.Theodoropoulos. *Comput. Chem. Eng.* **2002**, *26*, 641–963.

[87] Matsumoto, M.; Saito, S.; Ohmine, I. *Nature* **2002**, *416*, 409–413.

[88] Martonak, R.; Laio, A.; Bernasconi, M. *Z. Krystallogr.* **2005**, *220*, 489–498.

[89] Raiteri, P.; MArtonak, R.; Parrinello, M. *Angew. Chem. Int. Ed.* **2005**, *44*, 3769–3773.

[90] Clay, C.; Hodgson, A. *Curr. Opin. Solid State Mater. Sci.* **2005**, *9*, 11–18.

[91] Taylor, C. D.; Neurock, M. *Curr. Opin. Solid State Mater. Sci.* **2005**, *9*, 49–65.

[92] Meng, S.; Xu, L. F.; Wang, E. G.; Gao, S. *Phys. Rev. Lett.* **2002**, *89(17)*, 176104(4).

[93] Meng, S.; Wang, E. G.; Gao, S. *Phys. Rev. B* **2004**, *69*, 195404(13).

[94] Michaelides, A.; Ranea, V. A.; de Andres, P. L.; King, D. A. *Phys. Rev. Lett.* **2003**, *90(21)*, 216102(4).

[95] Ranea, V. A.; Michaelides, A.; Ramírez, R.; Vergés, J. A.; de Andres, P. L.; King, D. A. *Phys. Rev. B* **2004**, *69(20)*, 205411(9).

[96] Sebastiani, D.; delle Site, L. *J. Chem. Theor. Comput.* **2005**, *1*, 78–82.

[97] Cerdá, J.; Michaelides, A.; Bocquet, M.-L.; Feibelman, P. J.; Mitsui, T.; Rose, M.; Formin, E.; Salmeron, M. *Phys. Rev. Lett.* **2004**, *93(11)*, 116101(4).

[98] Haq, S.; Clay, C.; Darling, G. R.; Zimbitas, G.; Hodgson, A. *Phys. Rev. B* **2006**, *73(11)*, 115414(11).

[99] Ren, J.; Meng, S. *J. Am. Chem. Soc.* **2006**, *128*, 9282–9283.

[100] Ludwig, R. *Angew. Chem. Int. Ed.* **2003**, *42*, 3458–3460.

[101] Feibelman, P. J. *Phys. Rev. Lett.* **2003**, *90(18)*, 186103(4).

[102] Doering, D. L.; Madey, T. E. *Surf. Sci.* **1982**, *123*, 305–337.

[103] Feibelman, P. J. *Science* **2002**, *295*, 99–102.

[104] Michaelides, A.; Alavi, A.; King, D. A. *Phys. Rev. B* **2004**, *69*, 113404(4).

[105] Glebov, A.; Graham, A. P.; Menzel, A.; Toennis, J. P. *J. Chem. Phys.* **1997**, *106(22)*, 9382–9385.

[106] Ogasawara, H.; Yoshinobu, J.; Kawai, M. *J. Chem. Phys.* **1999**, *111(15)*, 7003–7009.

[107] Glebov, A. L.; Graham, A. P.; A.Menzel. *Surf. Sci.* **1999**, *427-428*, 22–26.

[108] Stevenson, K. P.; Kimmel, G. A.; Dohnàlek, Z.; Smith, R. S.; Kay, B. D. *Science* **1999**, *283*, 1505–1507.

[109] Morgenstern, M.; Müller, J.; Michely, T.; G.Comsa. *Zeitschrift für Physikalische Chemie* **1997**, *198*, 43–72.

[110] Haq, S.; Harnett, J.; Hodgson, A. *Surf. Sci.* **2002**, *505*, 171–182.

[111] Lilach, Y.; Iedema, M. J.; Cowin, J. P. *Phys. Rev. Lett.* **2007**, *98(1)*, 016105.

[112] Sexton, B. A. *Surf. Sci.* **1980**, *94*, 435–445.

[113] Fisher, G. B.; Gland, J. L. *Surf. Sci.* **1980**, *94*, 446–455.

[114] Ogasawara, H.; Brena, B.; Nordlund, D.; Nyberg, M.; A. Pelmenschikov, L. P.; Nilsson, A. *Phys. Rev. Lett.* **2002**, *89(27)*, 276102(4).

[115] Ogasawara, H.; Yoshinobu, J.; Kawai, M. *Chem. Phys. Lett.* **1994**, *231*, 188–192.

[116] Fisher, G. B.; Sexton, B. A. *Phys. Rev. Lett.* **1980**, *44(10)*, 683–687.

[117] Creighton, J. R.; White, J. M. *Surf. Sci.* **1982**, *122*, L648–L652.

[118] Völkening, S.; Berürftig, K.; Jacobi, K.; Wintterlin, J.; Ertl, G. *Phys. Rev. Lett.* **1999**, *83(13)*, 2672–2676.

[119] Bedürftig, K.; Völkening, S.; Wang, Y.; Wintterlin, J.; Jacobi, K.; Ertl, G. *J. Chem. Phys.* **1999**, *111(24)*, 11147–11154.

[120] Clay, C.; Haq, S.; Hodgson, A. *Phys. Rev. Lett.* **2004**, *92(4)*, 046102(4).

[121] Held, G.; Clay, C.; Barrett, S. D.; Haq, S.; Hodgson, A. *J. Chem. Phys.* **2005**, *123(6)*, 064711(7).

[122] Feibelman, P. J. *Phys. Rev. Lett.* **2003**, *91(5)*, 059601(1).

[123] Meng, S. *Surf. Sci.* **2005**, *575*, 300–306.

[124] Starke, U.; Heinz, K.; Materer, N.; Wander, A.; Michil, M.; Döll, R.; Hove, M. A. V.; Somorjai, G. A. *J. Vac. Sci. Technol. A* **1992**, *10(4)*, 2521–2528.

[125] Morgenstern, M.; Michely, T.; Comsa, G. *Phys. Rev. Lett.* **1996**, *77(4)*, 703(4).

[126] Harnett, J.; Haq, S.; Hodgson, A. *Surf. Sci.* **2003**, *528*, 15–19.

[127] Su, X.; Lianos, L.; Shen, Y. R.; Somorjai, G. A. *Phys. Rev. Lett.* **1998**, *80(7)*, 1533(4).

[128] Döbereiner, J. W. *Schweugg. J.* **1823**, *39*, 1.

[129] Berzelius, J. J. *Jber. Chem.* **1837**, *15*, 237.

[130] Smith, J. N.; Palmer, R. L. *J. Chem. Phys.* **1972**, *56*, 13.

[131] Anton, A. B.; Cadogan, D. C. *Surf. Sci.* **1990**, *239*, L548.

[132] Ogle, K. M.; White, J. M. *Surf. Sci.* **1984**, *139*, 43.

[133] Michaelides, A.; Hu, P. *J. Am. Chem. Soc.* **2001**, *123*, 4235–4242.

[134] Michaelides, A.; Hu, P. *J. Chem. Phys.* **2001**, *114(1)*, 513–519.

[135] Karlberg, G. S.; Olsson, F. E.; Persson, M.; Wahnström, G. *J. Chem. Phys.* **2003**, *119(9)*, 4865–4872.

[136] Jacob, T.; III, W. A. G. *J. Am. Chem. Soc.* **2004**, *126*, 9360–9368.

[137] Zimbitas, G.; Haq, S.; Hodgson, A. *J. Chem. Phys.* **2005**, *123(17)*, 174701(9).

[138] Zimbitas, G.; Hodgson, A. *Chem. Phys. Lett.* **2006**, *417*, 1–5.

[139] Takaoka, T.; Inamura, M.; Yanagimachi, S.; Kusunoki, I.; Komeda, T. *J. Chem. Phys.* **2004**, *121(9)*, 4331–4338.

[140] Dohnàlek, Z.; Kimmel, G. A.; Ciolli, R. L.; Stevenson, K. P.; Smith, R. S.; Kay, B. D. *J. Chem. Phys.* **2000**, *112(13)*, 5932–5941.

[141] Kimmel, G. A.; Petrik, N. G.; Dohnàlek, Z.; Kay, B. D. *Phys. Rev. Lett.* **2005**, *95(16)*, 166102(4).

[142] Kimmel, G. A.; Petrik, N. G.; Dohnàlek, Z.; Kay, B. D. *J. Chem. Phys.* **2006**, *125(4)*, 044713(12).

[143] Kimmel, G. A.; Petrik, N. G.; Dohnàlek, Z.; Kay, B. D. *J. Chem. Phys.* **2007**, *126(11)*, 114702(10).

[144] Nordlung, D.; Ogasawara, H.; Wernet, P.; Nyberg, M.; Odelius, M.; Pettersson, L. G. M.; Nilsson, A. *Chem. Phys. Lett.* **2004**, *395*, 161–165.

[145] Iedema, M. J.; Dresser, M. J.; Doering, D. L.; Rowland, J. B.; Hess, W. P.; Tsekouras, A. A.; P.Cowin, J. *J. Phys. Chem. B* **1998**, *102*, 9203–9214.

[146] Holloway, S.; Bennemann, K. H. *Surf. Sci.* **1980**, *101*, 327–333.

[147] Vassilev, P.; van Santen, R. A.; Koper, M. T. M. *J. Chem. Phys.* **2005**, *122*, 054701(12).

[148] Karlberg, G. S.; Wahnström, G. *Phys. Rev. Lett.* **2004**, *92(13)*, 136103(4).

[149] Badiali, J. P. *Molecular Physics* **1985**, *55*, 939.

[150] Jonsson, B. *Chem. Phys. Lett.* **1981**, *82*, 520–525.

[151] Christou, N. I.; Whitehouse, J. S.; Nicholson, D.; Parsonage, N. G. *J. Chem. Soc. Faraday Symp.* **1981**, *16*, 139–149.

[152] Lee, C. Y.; McCammon, J. A.; Rossky, P. J. *J. Chem. Phys.* **1984**, *80*, 4448–4455.

[153] Barbarino, G.; Gavotti, C.; Marchesi, M. *Chem. Phys. Lett.* **1984**, *104*, 478–484.

[154] Sonnenschein, A.; Heinzinger, K. *Chem. Phys. Lett.* **1983**, *102*, 550–554.

[155] Spohr, E.; Heinzinger, K. *Chem. Phys. Lett.* **1986**, *123(3)*, 218–221.

[156] Spohr, E. *J. Phys. Chem.* **1989**, *93*, 6171–6180.

[157] Nagy, G.; Heinzinger, K.; Spohr, E. *Faraday Discuss.* **1992**, *94*, 307–315.

[158] Foster, K.; Raghavan, K.; Berkowitz, M. *Chem. Phys. Lett* **1989**, *162(2)*, 32–38.

[159] Raghavan, K.; Foster, K.; Motakabbir, K.; Berkowitz, M. *J. Chem. Phys.* **1991**, *94(3)*, 2110–2117.

[160] Raghavan, K.; Foster, K.; Berkowitz, M. *Chem. Phys. Lett.* **1991**, *177*, 426–432.

[161] Xia, X.; Perera, L.; Essmann, U.; Berkowitz, M. *Surf. Sci.* **1995**, *335*, 401–415.

[162] Yeh, I.-C.; Berkowitz, M. *J. Chem. Phys.* **1999**, *111(7)*, 3155–3162.

[163] Xia, X.; Berkowitz, M. *Phys. Rev. Lett* **1995**, *74(16)*, 3193–3197.

[164] Henschel, H.; Krämer, T.; Lankau, T. *Langmuir* **2006**, *22*, 10942–10950.

[165] Witek, H.; Buch, V. *J. Chem. Phys.* **1999**, *110(6)*, 3168–3175.

[166] Nutt, D. R.; Stone, A. J. *Langmuir* **2004**, *20*, 8715–8720.

[167] Okawa, S.; Saito, A.; Matsui, T. *Int. J. Refrig.* **2006**, *29*, 134–141.

[168] Lankau, T.; Nagorny, K.; Cooper, I. L. *Langmuir* **1999**, *15*, 7308–7315.

[169] Lankau, T.; Cooper, I. L. *J. Phys. Chem. A* **2001**, *105*, 4084–4095.

[170] Lankau, T. *J. Phys. Chem. A* **2002**, *106*, 6154–6160.

[171] Konrad, O.; Lankau, T. *Chem. Phys. Lett.* **2002**, *359*, 35–40.

[172] Andreussi, O.; Donadio, D.; Parrinello, M.; Zewail, A. H. *Chem. Phys. Lett.* **2006**, *426*, 115.

[173] Alavi, A.; Kohanoff, J.; Parrinello, M.; Frenkel, D. *Phys. Rev. Lett.* **1994**, *73*, 2599.

[174] Perdew, J. P.; Burke, K.; Ernzerhof, M. *Phys. Rev. Lett.* **1996**, *77*, 3865.

[175] Jacobi, K.; Bedürftig, K.; Wang, Y.; Ertl, G. *Surf. Sci.* **2001**, *472*, 9–20.